



CERN-EP-2021-200
09 September 2021

$K^*(892)^0$ and $\phi(1020)$ production in p–Pb collisions at $\sqrt{s_{NN}} = 8.16$ TeV

ALICE Collaboration*

Abstract

The production of $K^*(892)^0$ and $\phi(1020)$ resonances has been measured in p–Pb collisions at $\sqrt{s_{NN}} = 8.16$ TeV using the ALICE detector. Resonances are reconstructed via their hadronic decay channels in the rapidity interval $-0.5 < y < 0$ and the transverse momentum spectra are measured for various multiplicity classes up to $p_T = 20$ GeV/ c for $K^*(892)^0$ and $p_T = 16$ GeV/ c for $\phi(1020)$. The p_T -integrated yields and mean transverse momenta are reported and compared with previous results in pp, p–Pb and Pb–Pb collisions. The x_T scaling for $K^*(892)^0$ and $\phi(1020)$ resonance production is newly tested in p–Pb collisions and found to hold in the high- p_T region at LHC energies. The nuclear modification factors (R_{pPb}) as a function of p_T for K^{*0} and ϕ at $\sqrt{s_{NN}} = 8.16$ TeV are presented along with the new R_{pPb} measurements of K^{*0} , ϕ , Ξ , and Ω at $\sqrt{s_{NN}} = 5.02$ TeV. At intermediate p_T (2–8 GeV/ c), R_{pPb} of Ξ , Ω show a Cronin-like enhancement, while K^{*0} and ϕ show no or little nuclear modification. At high p_T (> 8 GeV/ c), the R_{pPb} values of all hadrons are consistent with unity within uncertainties. The R_{pPb} of $K^*(892)^0$ and $\phi(1020)$ at $\sqrt{s_{NN}} = 8.16$ and 5.02 TeV show no significant energy dependence.

arXiv:2110.10042v1 [nucl-ex] 19 Oct 2021

*See Appendix A for the list of collaboration members

1 Introduction

High-energy heavy-ion (A–A) collisions provide a unique opportunity to study the deconfined quark–gluon plasma (QGP) created in such collisions [1–3]. The hot and dense medium created in heavy-ion collisions evolves with time and cools down to form a phase where hadron resonance gas is studied. Evidence at RHIC and the LHC suggest that the QGP phase is followed by a hadronic phase where the hadrons interact via rescattering and regeneration processes, before the final freeze-out. Resonances are short-lived hadrons that decay via the strong interactions. They play an important role to understand the particle production mechanisms and for the characterization of the dynamic evolution of the system formed in heavy-ion collisions. They are used as a sensitive probe of the hadronic phase, where their mass, width and yield could be modified due to interaction of their decay products through re-scattering and regeneration processes [4–15]. ALICE has previously measured $K^*(892)^0$ and $\phi(1020)$ production in pp collisions at $\sqrt{s} = 5.02, 7, 8$ and 13 TeV [16–22], in p–Pb collisions at $\sqrt{s_{NN}} = 5.02$ TeV [23] and Pb–Pb collisions at $\sqrt{s_{NN}} = 2.76$ and 5.02 TeV [13, 15, 18, 19].

Proton–lead collisions are intermediate between pp and Pb–Pb collisions in terms of the size of the colliding system and the produced particle multiplicities. Recent measurements in high–multiplicity pp, p–Pb and d–Au collisions at different energies have uncovered strong flow-like effects even in these small collision systems [14, 22–25], whose origin is not fully understood. To investigate the mechanism of particle production and the origin of these effects, the ALICE Collaboration has studied the multiplicity dependence of light–flavor particle production for many species like π^\pm , K^\pm , K_S^0 , $K^*(892)^0$, $\phi(1020)$, Λ , $\Lambda(1520)$, $\Sigma^{*\pm}$, Ξ^\pm , Ξ^{*0} , Ω^\pm in p–Pb collisions at $\sqrt{s_{NN}} = 5.02$ TeV [23, 26–29] and in pp collisions at $\sqrt{s} = 7$ and 13 TeV [17, 20, 22, 30]. This paper reports on the multiplicity dependence of $K^*(892)^0$ and $\phi(1020)$ meson production at the highest center-of-mass energy, $\sqrt{s_{NN}} = 8.16$ TeV, reached at the LHC in p–Pb collisions. This provides an opportunity to extend the previous studies of production of these particles in p–Pb collisions at $\sqrt{s_{NN}} = 5.02$ TeV [23] to a higher multiplicity reach and a larger p_T coverage. Hadron production is governed by the soft and hard scattering processes at LHC energies. The bulk of particles produced in high energy collisions is dominated by low transverse momentum particles from soft interactions, which are non-perturbative in nature. The yield of particles at low p_T is not well understood from the first principles of QCD and their description relies on phenomenological QCD-based models such as EPOS-LHC, DPMJET and HIJING. The measurements in the low-momentum region of the spectra presented in this article provide input for the tuning of these event generators. In this paper, measurements of $K^*(892)^0$ and $\phi(1020)$ are compared with predictions from EPOS-LHC [31], DPMJET [32] and HIJING [33].

The transverse momentum spectra of light–flavor hadrons have shown a clear evolution with multiplicity in high energy pp and p–Pb collisions [17, 22, 23, 26, 34], similar to that observed in Pb–Pb collisions [13, 18, 19, 35, 36], where in the latter case the effect is usually attributed to a collective expansion of the system. The increase in slope of the p_T spectra as a function of multiplicity attributed to the radial flow is related to the low- p_T region of the spectrum, where flow is relevant. This feature is also reflected in an increase of the average transverse momentum $\langle p_T \rangle$ with multiplicity. In contrast to the yields dN/dy , which evolve smoothly as a function of multiplicity for different collision systems, the $\langle p_T \rangle$ of light–flavour hadrons as well as $K^*(892)^0$ and $\phi(1020)$, rises faster as a function of multiplicity in pp and p–Pb collisions than in Pb–Pb collisions, as discussed in Refs. [20, 22, 23]. The new measurements, with the highest multiplicity reach in p–Pb collisions, and comparison with the different model predictions can be used to further extend these studies.

The high- p_T particle production is analyzed within the framework of perturbative Quantum Chromodynamics (pQCD) which features a nearly scale-invariant behavior of elementary parton–parton hard-scattering processes [37, 38]. The convolution of hard scattering cross sections with the parton distribution functions (PDFs) of incident hadrons and fragmentation functions (FFs) leads to the observed scaling of the inclusive invariant cross section $Ed^3\sigma/dp^3$ as p_T^{-n} at fixed transverse x , $x_T = 2p_T/\sqrt{s}$ [39, 40].

The exponent n can be related to the scattering processes in which high- p_T hadrons are produced. If hadrons are produced by leading twist (LT) $2 \rightarrow 2$ hard subprocesses, $n \sim 4$ and for higher twist (HT) processes, $n \sim 8$. It has been observed that the exponent value decreases with increasing collision energy, which suggests that the contribution of higher twist processes on high- p_T hadron production is reduced as a function of energy. The transverse momentum distributions of different particle species at high p_T are observed to satisfy a universal x_T scaling over a wide energy range up to $\sqrt{s} = 13$ TeV. This scaling behavior was observed by the CDF [41, 42] and UA1 [43] Collaborations in $p(\bar{p})$ collisions, and by the STAR [44], ALICE [45] and CMS [46] Collaborations in pp collisions. In this paper, the x_T scaling of $K^*(892)^0$ and $\phi(1020)$ mesons are tested in p–Pb collisions at LHC energies. The transverse momentum distributions of the particles in p–Pb collisions are compared to those in pp collisions using the nuclear modification factor (R_{pPb}). The measurement of R_{pPb} acts as a control experiment observable in p–Pb collisions [47] in the context of the observed high- p_T hadron suppression in Pb–Pb collisions [15]. In this paper, R_{pPb} measurements of $K^*(892)^0$ and $\phi(1020)$ in p–Pb collisions at $\sqrt{s_{NN}} = 5.02$ and 8.16 TeV, and that of Ξ and Ω in p–Pb collisions at 5.02 TeV are reported. Similar measurements are also reported for strange and multi-strange hadrons by CMS [48], and for π^\pm , K^\pm and $p(\bar{p})$ by ALICE [26] in p–Pb collisions at $\sqrt{s_{NN}} = 5.02$ TeV. At high p_T (> 8 GeV/ c), the values of R_{pPb} for all light hadrons are similar and found to be consistent with unity within the uncertainties. At intermediate p_T ($2 < p_T < 8$ GeV/ c), the values of R_{pPb} for strange baryons (Ξ , Ω) show an enhancement with a clear mass dependence [48]. One of the explanations for this enhancement, known as the Cronin effect is due to multiple scattering of the projectile partons with partons of nucleons inside the target nucleus [49]. Alternatively, the enhancement of the R_{pPb} is described by parton recombination models [50] as a final state effect. In this paper, the particle species and collision energy dependence of R_{pPb} is studied for p–Pb collisions at LHC energies.

Throughout this paper, the results for $K^*(892)^0$ and $\bar{K}^*(892)^0$ are averaged and denoted by the symbol K^{*0} , while $\phi(1020)$ is denoted by ϕ . The paper is organized as follows. In section 2, the dataset, event and track selection criteria, the analysis techniques, the procedure for extraction of the yields and the study of the systematic uncertainties are briefly discussed. In section 3, the results on the transverse momentum spectra, the dN/dy , $\langle p_T \rangle$, x_T scaling and R_{pPb} in p–Pb collisions at $\sqrt{s_{NN}} = 8.16$ TeV are presented. Finally, the results are summarized in section 4.

2 Data analysis

The measurements of K^{*0} and ϕ meson production in p–Pb collisions at $\sqrt{s_{NN}} = 8.16$ TeV have been performed on data collected with the ALICE detector in the year 2016. The resonances are reconstructed via their hadronic decay channels with branching ratios (BR) of 66.6% for $K^{*0} \rightarrow \pi^\pm K^\mp$ and 49.2% for $\phi \rightarrow K^+ K^-$ in the rapidity interval $-0.5 < y < 0$, where y stands for the rapidity in the nucleon–nucleon center-of-mass. For both K^{*0} and ϕ , the analysis is performed in various multiplicity classes and also using a multiplicity-integrated sample.

2.1 Event selection

The detailed description of the ALICE detector setup and its performance can be found in Refs. [51, 52]. In p–Pb configurations, the ^{208}Pb beam circulates towards the positive z -direction in the ALICE laboratory frame, while the proton beam circulates in the opposite direction. Due to the asymmetric system, the center-of-mass frame is shifted in the rapidity by $\Delta y = -0.465$ in the direction of the proton beam with respect to the laboratory frame. The minimum bias trigger was configured to select events by requiring at least a coincidence signal in both the V0A and V0C detectors [53, 54]. The V0 detector system consists of two arrays of 32 scintillator detectors, one on each side of the interaction point covering the full azimuthal angle in the pseudorapidity regions $2.8 < \eta < 5.1$ (V0A) and $-3.7 < \eta < -1.7$ (V0C).

Table 1: Mean charged particle multiplicity densities ($\langle dN_{ch}/d\eta \rangle$) measured in pseudorapidity range $|\eta_{lab}| < 0.5$, corresponding to the various multiplicity classes defined using the V0A detector in p–Pb collisions at $\sqrt{s_{NN}} = 8.16$ TeV [54].

V0A percentile (%)	$\langle dN_{ch}/d\eta \rangle_{ \eta_{lab} < 0.5}$
0–5	53.22 ± 1.38
5–10	42.40 ± 1.10
10–20	35.49 ± 0.92
20–40	26.89 ± 0.70
40–60	18.39 ± 0.48
60–80	10.97 ± 0.29
80–100	4.47 ± 0.14

The background events due to beam–gas interaction and other machine-induced background collisions are rejected using the timing information from the V0 and the Zero Degree Calorimeter (ZDC) [52]. The primary vertex of a collision is determined using charged tracks reconstructed in the Inner Tracking System (ITS) [55] and the Time Projection Chamber (TPC) [56]. The events are selected whose primary vertex position along the beam axis (v_z , z is the longitudinal direction) is within ± 10 cm from the nominal interaction point. Pile-up events from the triggered bunch crossing are rejected if multiple collision vertices are identified in the Silicon Pixel Detector (SPD), which is the innermost detector of the ITS [52, 56]. The total number of events analyzed after applying the event selection criteria is about 30 million. The minimum bias events are further divided into seven multiplicity classes, according to the total charge deposited in the forward V0A detector [53]. The yield of K^{*0} and ϕ are measured in the rapidity interval $-0.5 < y < 0$ for the following event multiplicity classes, 0–5%, 5–10%, 10–20%, 20–40%, 40–60%, 60–80% and 80–100%. The p_T spectra normalized to the fraction of non-single-diffractive (NSD) events are also obtained for both K^{*0} and ϕ . The mean charged-particle multiplicity ($\langle dN_{ch}/d\eta \rangle$) corresponding to each multiplicity class, and measured in the pseudorapidity interval $|\eta_{lab}| < 0.5$, is given in Table 1 taken from [54].

2.2 Track selection and particle identification

The charged tracks coming from the primary vertex are selected in the pseudorapidity interval $|\eta| < 0.8$ with $p_T > 0.15$ GeV/ c . This ensures the uniform acceptance for the central barrel detectors. The high quality tracks are chosen based on selection criteria as done previously in Ref. [23]. The K^{*0} and ϕ mesons are reconstructed from the charged tracks which have crossed at least 70 out of maximum 159 horizontal segments along the transverse readout plane of the TPC. The contamination from secondary particles originating from weak decays and beam background events are reduced by applying a selection on the distance of closest approach to the primary vertex in the transverse plane (DCA_{xy}) and along the longitudinal direction (DCA_z). A p_T -dependent cut of $DCA_{xy}(p_T) < (0.0105 + 0.035 p_T^{-1.1})$ cm, with p_T in GeV/ c , is used, which is less than 7 times its resolution. The track DCA_z is required to be less than 2 cm [57]. The decay daughters (pions and kaons) of resonances are identified by measuring the specific ionization energy loss (dE/dx) in the detector gas of the TPC and their time-of-flight information using the TOF [58]. The dE/dx resolution of the TPC is denoted as σ_{TPC} and the charged tracks are identified as pions and kaons if the mean specific energy loss measured by the TPC is within $6\sigma_{TPC}$, $3\sigma_{TPC}$ and $2\sigma_{TPC}$ from the expected $\langle dE/dx \rangle$ values in the momentum range $p < 0.3$ GeV/ c , $0.3 < p < 0.5$ GeV/ c and $p > 0.5$ GeV/ c , respectively. In addition to the TPC, if the TOF information is available, the charged tracks are identified by requiring the time-of-flight values within $3\sigma_{TOF}$ of the expected values for the full momentum range.

2.3 Yield extraction

The K^{*0} and ϕ resonances are reconstructed from their decay products using the invariant mass technique. The invariant mass distributions are obtained from unlike charge πK (for K^{*0}) and KK (for ϕ) pairs in the same event. The distributions exhibit a signal peak and a large combinatorial background from the uncorrelated πK (KK) pairs. The combinatorial background is estimated using two methods, mixed-event and like-sign. In the mixed-event method, the tracks from one event are paired with oppositely charged tracks from other events. Each event is mixed with five other events to reduce the contribution of statistical uncertainty from the background distribution. The events which are mixed are selected to have similar characteristics like the longitudinal position of primary vertex (v_z) must differ by less than 1 cm and the multiplicity percentiles computed using the V0A amplitude must differ by less than 5%. The mixed-event distributions for K^{*0} (ϕ) are normalized in the mass region $1.1 < m_{inv} < 1.15$ GeV/ c^2 ($1.04 < m_{inv} < 1.15$ GeV/ c^2). In the like-sign method, tracks of identical charges from the same events are paired and the invariant mass distribution for the uncorrelated background is obtained as the geometric mean $2\sqrt{n^{++} \times n^{--}}$, where n^{++} and n^{--} are the number of positive-positive and negative-negative pairs in each invariant mass bin, respectively. The mixed-event technique is the default method used for the extraction of yield both for K^{*0} and ϕ whereas the like-sign background is used for the estimation of the systematic uncertainty. In Fig. 1, panels (a) and (b) show the invariant mass distributions of π^+K^\pm and K^+K^- pairs from the same events and the mixed-events in the transverse momentum interval $1.4 \leq p_T < 1.6$ and $0.6 \leq p_T < 0.8$ GeV/ c for 0–100% in p–Pb collisions, respectively. The π^+K^\pm and K^+K^- invariant mass distributions after mixed-event background subtraction

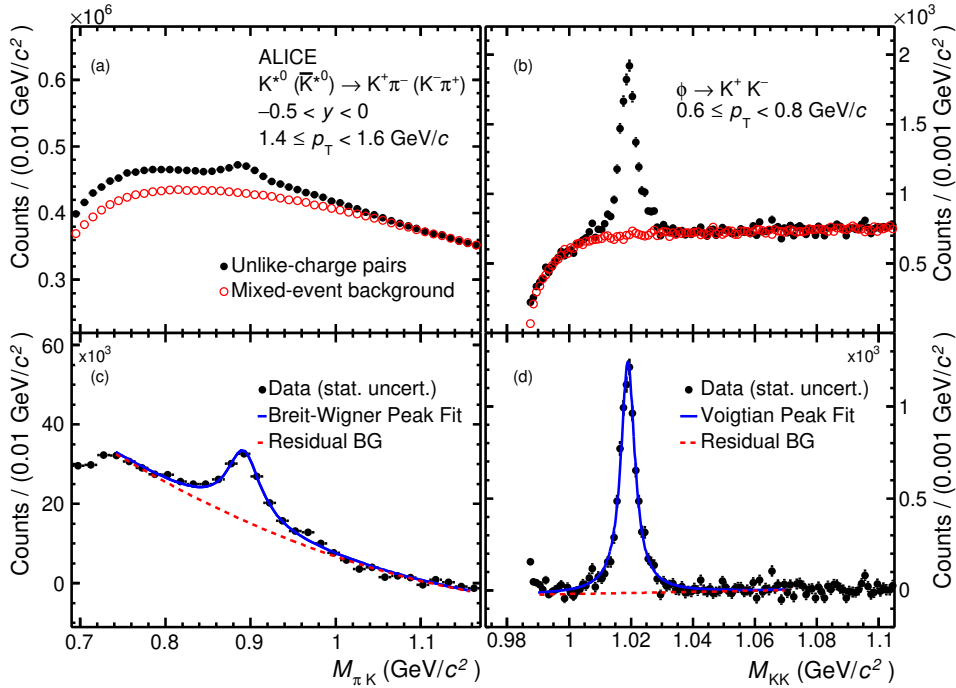


Figure 1: Invariant mass distributions for K^{*0} and ϕ in the multiplicity class 0–100% and transverse momentum range $1.4 \leq p_T < 1.6$ GeV/ c and $0.6 \leq p_T < 0.8$ GeV/ c , respectively. In the upper panels, (a) and (b), black markers show the unlike-sign invariant mass distributions and red markers show the normalized mixed event background. After the background subtraction the signals are shown in the lower panels (c) and (d). The K^{*0} peak is described by a Breit-Wigner function whereas the ϕ peak is fitted with a Voigtian function. The residual background is described by the 2nd order polynomial function.

are shown in panels (c) and (d) of Fig. 1, respectively, where the characteristic signal peak is observed

on top of the residual background. The residual background arises due to correlated pairs from jets, misidentification of the decay daughters of resonances and decay of other particles [23]. The raw yields of resonances are extracted in each p_T bin and multiplicity class. The signal peak is fitted with a Breit-Wigner and a Voigtian function (convolution of Breit-Wigner and Gaussian functions) for K^{*0} and ϕ , respectively. A second order polynomial function is used to describe the shape of the residual background for both resonances. The signal peak fit is performed in the range $0.75 < M_{K\pi} < 1.15$ GeV/ c^2 ($0.99 < M_{KK} < 1.07$ GeV/ c^2) for K^{*0} (ϕ). The widths of the K^{*0} and ϕ are fixed to their PDG values $\Gamma(K^{*0}) = 47.4 \pm 0.6$ MeV/ c^2 , $\Gamma(\phi) = 4.26 \pm 0.04$ MeV/ c^2 [59], whereas the resolution parameter of the Voigtian function for ϕ is kept as a free parameter. The measured resolution of the ϕ mass as a function of p_T (σ of Gaussian) varies between 1 and 3 MeV/ c^2 . The sensitivity to the choice of the fitting range, the normalization interval, the shape of the background function, the width and resolution parameters has been studied by varying the default settings, as described in section 3.1. In minimum bias collisions, K^{*0} (ϕ) production is measured in the p_T range from 0 to 20 GeV/ c (0.4 to 16 GeV/ c). With the available data samples, K^{*0} production is measured up to $p_T = 15$ GeV/ c in 0–5% and 5–10%, up to $p_T = 20$ GeV/ c in 10–20%, 20–40% and 40–60%, up to 10 GeV/ c in 60–80% and up to 6 GeV/ c in 80–100% multiplicity classes, while the ϕ production is measured up to $p_T = 16$ GeV/ c in 0–5%, 5–10%, 10–20%, 20–40%, $p_T = 12$ GeV/ c in 40–60%, $p_T = 10$ GeV/ c in 60–80% and $p_T = 6$ GeV/ c in 80–100% multiplicity class. The raw transverse momentum distributions are normalized by the number of accepted events and corrected for the branching ratio, detector acceptance and reconstruction efficiency ($A \times \epsilon_{rec}$), signal loss and inefficiency in trigger selection and primary vertex reconstruction. The $A \times \epsilon_{rec}$ is obtained from the Monte Carlo simulation (MC) based on the DPMJET [32] event generator and the interaction of the generated particles passing through the ALICE detector geometry is modeled using GEANT3 [60]. It is defined as the ratio of the reconstructed K^{*0} (ϕ) to the generated K^{*0} (ϕ), both in the rapidity interval $-0.5 < y < 0$, and determined as a function of p_T . The same track and particle identification (PID) selection criteria are applied to the decay daughter of resonances in MC as are used in the analysis. The shape of the generated p_T distributions are different from the measured p_T distributions, therefore a re-weighting procedure is used, in which the generated distributions are weighted to match the measured distributions. The effect of the re-weighting procedure on $A \times \epsilon_{rec}$ is $\sim 2 - 5\%$ at low p_T (< 1 GeV/ c) and negligible for $p_T > 1$ GeV/ c . The re-weighted $A \times \epsilon_{rec}$ is used to correct the raw p_T distribution. No significant multiplicity dependence of $A \times \epsilon_{rec}$ is observed, therefore the raw p_T spectra in the various multiplicity classes are corrected with the minimum bias $A \times \epsilon_{rec}$ values. The signal loss corrections that account for the loss in K^{*0} and ϕ yields caused by the event selection with minimum bias trigger, rather than all NSD events, are found to be negligible in the measured p_T range. The correction factor due to the vertex reconstruction efficiency is negligible in all multiplicity classes. The minimum bias p_T spectra are normalized to the fraction of NSD events, which is 0.992.

2.4 Systematic uncertainties

The sources of systematic uncertainties of the measurement of K^{*0} and ϕ production are signal extraction, track selection criteria, particle identification, global tracking efficiency, uncertainty in the material budget of the ALICE detector and the hadronic interaction cross section in the detector material. A similar approach is adopted as used for the systematic uncertainty study of K^{*0} and ϕ in p–Pb collisions at $\sqrt{s_{NN}} = 5.02$ TeV [23]. No multiplicity dependence of the systematic effects is observed, therefore the systematic uncertainties of minimum bias p_T spectra are propagated for all multiplicity event classes studied. A summary of systematic uncertainties for K^{*0} (ϕ) in two transverse momentum intervals, $0 < p_T < 4$ GeV/ c ($0.4 < p_T < 4$ GeV/ c) and $4 < p_T < 20$ GeV/ c ($4 < p_T < 16$ GeV/ c) are given in Table 2. The uncertainties due to signal extraction include variations of the signal peak fitting range, variations of width and mass resolution, mixed–event background normalization region, choice of residual background function and combinatorial background. The fitting range of the πK (KK) invariant mass distribution is varied by ~ 50 (5) MeV/ c^2 on each side of the signal peak. The normalization range of the πK (KK) invariant mass distributions differed by approximately 150 (50) MeV/ c^2 with respect to

Table 2: The sources of systematic uncertainties for K^{*0} and ϕ yields in p–Pb collisions at $\sqrt{s_{NN}} = 8.16$ TeV. For each source, the average uncertainties are listed for the low and high- p_T intervals.

Systematic variation	K^{*0}				ϕ	
	0.0–4.0	p_T (GeV/c)		0.4–4.0	4.0–16	
		4.0–20.0	4.0–20.0	4.0–20.0	4.0–16	
Yield extraction (%)	7.5	8.0	2.8	4.5		
Track selection (%)	3.0	2.0	4.4	5.5		
Particle identification (%)	4.3	5.0	1.9	3.5		
Global tracking efficiency (%)	2.0	3.2	2.0	2.3		
Material budget (%)	1.2	<0.5	2.2	< 0.5		
Hadronic Interaction (%)	1.9	<0.5	2.4	< 1		
Total (%)	9.6	10.2	6.7	8.3		

the default value. The width of the resonances is fixed for the default fit whereas it is kept free for systematic studies. The residual background is fitted with a first-order and third-order polynomial function for the systematic studies of the signal extraction. For ϕ resonance, the effect of the variation of the resolution parameter (σ of the Gaussian) on the yield is also included in the systematic uncertainties. The combinatorial background from the like-sign method is used for systematic studies. The contribution of systematic uncertainties due to the signal extraction is 7.5–8% for K^{*0} and 2.8–4.5% for ϕ . The systematic effects due to the charged track selection are studied by varying the criteria based on the number of crossed readout rows in the TPC and the distance of closest approach to the primary vertex of the collision [57]. The relative contribution of uncertainties due to the track selection are 2–3 % for K^{*0} and about 4.4–5.5% for the ϕ . For the PID systematic uncertainty, the selections based on the TPC dE/dx and TOF time-of-flight are varied. Three variations are taken where one is a momentum dependent PID selection of $5\sigma_{\text{TPC}}$ ($0 < p < 0.3$), $2.5\sigma_{\text{TPC}}$ ($0.3 < p < 0.5$), $1.5\sigma_{\text{TPC}}$ ($p > 0.5$) with $3\sigma_{\text{TOF}}$, and two momentum-independent selection; $2\sigma_{\text{TPC}}$ with $3\sigma_{\text{TOF}}$ and $2\sigma_{\text{TPC}}$ only, for both K^{*0} and ϕ . This results in systematic uncertainties of 4.3–5% for K^{*0} and 1.9–3.5% for the ϕ . The uncertainty related to global tracking arises from the difference in the ITS-TPC track matching efficiency in data and MC. It is estimated from the single charged track uncertainty by taking the linear sum of the uncertainties of the two charged tracks which are used to reconstruct the resonances. It contributes to the systematic uncertainties with 2–3.2% and 2–2.3% for K^{*0} and ϕ , respectively. The material budget systematic effects account for the uncertainties in the estimation of the ALICE detector material budget and is estimated to be 1.2% for K^{*0} and 2.2% for ϕ at low p_T . It is negligible at $p_T > 4$ GeV/c for both K^{*0} and ϕ . The systematic uncertainty due to the hadronic interaction cross section in the detector material is estimated to be 1.9% for K^{*0} and 2.4% for ϕ at low p_T , and negligible for $p_T > 4$ GeV/c. For both the material budget and the hadronic interaction uncertainties, the effects are evaluated by combining the uncertainties of the two charged tracks (π , K for K^{*0} and two K for ϕ) determined in accordance with the kinematics of the decay. The systematic uncertainties of the material budget and the hadronic interaction cross section were taken from [23]. The total systematic uncertainties is taken as the quadratic sum of all contributions and varies as 9.6–10.2% for K^{*0} and 6.7–8.3% for ϕ . The sources of systematic uncertainties that are multiplicity-dependent and uncorrelated across different multiplicity classes are also estimated. The systematic uncertainties due to signal extraction and PID are fully uncorrelated, whereas global tracking, track selection criteria, material budget and hadronic cross section are correlated among event multiplicity classes.

3 Results and discussion

3.1 Transverse momentum spectra

The measurement of K^{*0} (ϕ) production performed in the rapidity interval $-0.5 < y < 0$ up to $p_T = 20$ (16) GeV/c in p-Pb collisions at $\sqrt{s_{NN}} = 8.16$ TeV is reported. Figure 2 shows p_T spectra of K^{*0} (left panel) and ϕ (right panel) for NSD events. These are compared with the predictions from EPOS-LHC [31, 61], DPMJET [32] and HIJING [33] models.

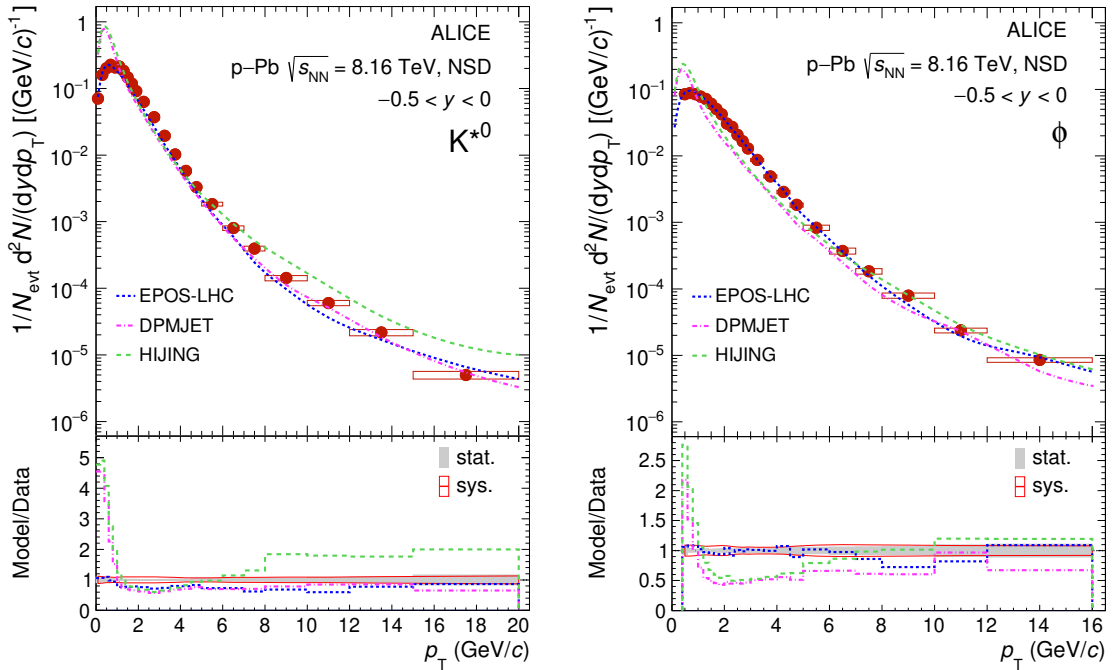


Figure 2: Top panels: Transverse momentum spectrum of K^{*0} (left) and ϕ (right) as a function of p_T for the NSD events, measured in the rapidity interval $-0.5 < y < 0$ for p-Pb collisions at $\sqrt{s_{NN}} = 8.16$ TeV. The statistical and systematic uncertainties are shown as bars and boxes, respectively. The NSD spectrum is compared with the predictions from EPOS-LHC [31, 61], DPMJET [32] and HIJING [33]. Bottom panels: The ratios of p_T spectra from model to data. The shaded bands around unity describe the statistical and systematic uncertainties of the data point.

The bottom panels of Fig. 2 show the ratios of p_T spectra from these models to the data. The EPOS Monte Carlo event generator is a hadronic interaction parton model based on Gribov’s Reggeon field theory formalism which includes the feature of collective hadronization and the core-corona mechanism from pp to A–A collisions [62–64]. If the string segments of the final state parton have high energy density that region is known as the “core”, whereas the region with strings of low energy density surrounding the core is called the “corona”. The core evolves hydrodynamically and subsequently hadronizes to form the bulk of the system whereas the strings in the corona region break through the production of quark-antiquark pairs, which hadronized as fragmentation processes in vacuum. EPOS-LHC [31] is a tune of EPOS1.99 [65] that incorporates a parameterization of flow based on LHC data. The EPOS1.99 model is different from EPOS2.x [66] and EPOS3.x [61] as it does not use the complete 3D hydro calculation followed by the hadronic cascade but instead relies on the fast covariant approach. It describes various

observables in the minimum bias heavy-ion collisions as well as small collision systems up to a few GeV/c at LHC energies. DPMJET is a QCD-inspired dual parton model based on the Gribov-Glauber approach that treats the soft and hard scattering interaction processes differently. HIJING combines the perturbative QCD process with soft excitation, the production of multiple minijets, the interactions of jets in dense hadronic matter, and nuclear shadowing of parton distribution functions. For the K^{*0} resonance, the EPOS-LHC model gives a good description in the measured p_T region whereas the DPMJET and HIJING models overestimate the data at low p_T (< 1 GeV/c) and underestimate for $1 < p_T < 8$ GeV/c. The EPOS-LHC model also describes the ϕ p_T spectrum relatively better than the DPMJET and HIJING for all p_T . The EPOS-LHC model, where a different parametrization of flow is introduced in small collision systems like pp than the large volume produced in heavy-ion collisions, gives a better description of the transverse momentum distributions for both K^{*0} and ϕ in p-Pb collisions.

Figure 3 shows the $\sqrt{s_{NN}}$ dependence of the transverse momentum spectra of K^{*0} and ϕ for NSD events in p-Pb collisions. The upper panels of Fig. 3 show a comparison of the transverse momentum spectra of K^{*0} and ϕ at $\sqrt{s_{NN}} = 5.02$ and 8.16 TeV whereas the lower panels show the ratio of the p_T -differential yield at $\sqrt{s_{NN}} = 8.16$ to 5.02 TeV and its comparison with the results obtained from models [31–33, 61]. The uncertainties of the ratios are obtained as the sum in quadrature of the uncertainties of the spectra at the two energies, which are largely uncorrelated. The differential yield ratio seems to be independent of p_T within systematic uncertainties and values are close to unity up to 1 GeV/c for both K^{*0} and ϕ . It suggests that the particle production in the soft scattering region is not strongly dependent on collision energy. The slope of the differential yield ratios increases as a function of p_T for $p_T \gtrsim 1$ GeV/c. Similar behavior is also observed in pp collisions in Ref. [21]. The p_T differential yield ratios obtained from EPOS-LHC, DPMJET, and HIJING are consistent with the measurements within the systematic uncertainties and reproduce well the energy dependence trend for K^{*0} and ϕ in p-Pb collisions.

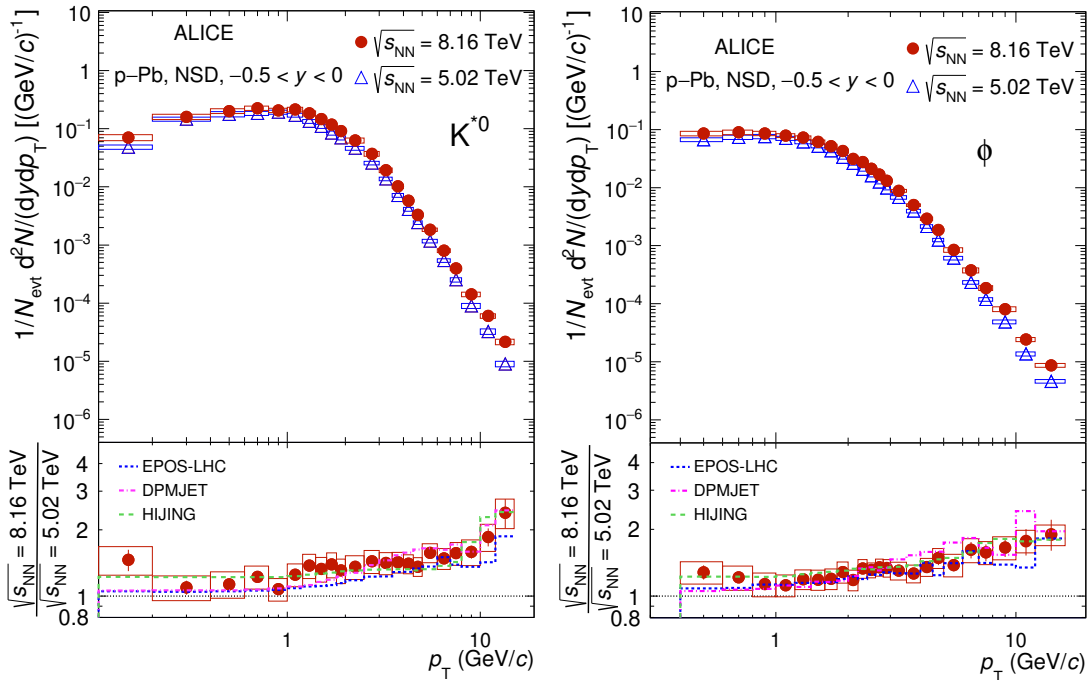


Figure 3: Top panels: Energy dependence comparison of the transverse momentum spectra of K^{*0} (left) and ϕ (right) as a function of p_T for the NSD events, measured in the rapidity interval $-0.5 < y < 0$ for p-Pb collisions at $\sqrt{s_{NN}} = 5.02$ and 8.16 TeV. Bottom panels: The ratio of p_T spectrum at $\sqrt{s_{NN}} = 8.16$ TeV to the p_T spectrum at $\sqrt{s_{NN}} = 5.02$ TeV. The ratio is compared with the predictions from EPOS-LHC [31, 61], DPMJET [32] and HIJING [33]. The statistical and systematic uncertainties are shown as bars and boxes, respectively.

Figure 4 shows the transverse momentum distributions of K^{*0} (left panel) and ϕ (right panel) in various multiplicity classes. The ratios of p_T spectra in various multiplicity classes to the p_T spectrum for NSD events are shown in the bottom panels of Fig. 4.

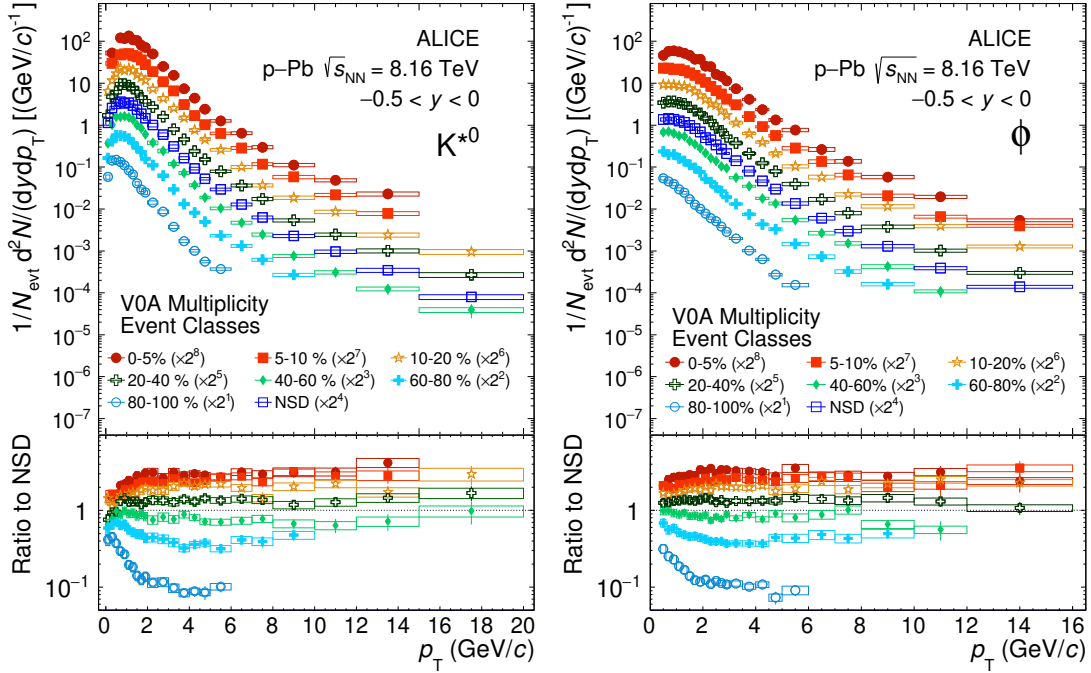


Figure 4: Top panels: The transverse momentum spectra of K^{*0} (left) and ϕ (right) for various multiplicity classes, measured in the rapidity interval $-0.5 < y < 0$ for p-Pb collisions at $\sqrt{s_{NN}} = 8.16$ TeV. Bottom panels: The ratios of p_T spectra of given event multiplicity classes to the NSD spectra are shown. The statistical and systematic uncertainties are shown as bars and boxes, respectively.

For $p_T \lesssim 4$ GeV/c, the slopes of the p_T spectra increase from low to high multiplicity classes, whereas the spectral shapes are similar at high p_T for all multiplicity classes. This indicates that processes like radial flow, which lead to a change in the shape of the p_T spectra for various multiplicity classes, dominate mainly at low p_T [36]. The increase in the slope of p_T spectrum with multiplicity is reflected in Fig. 5 for $\langle p_T \rangle$ as a function of multiplicity. A similar behavior was also observed for K^{*0} and ϕ in p-Pb collisions [23] at $\sqrt{s_{NN}} = 5.02$ TeV. The hardening of the p_T spectra with charged particle multiplicity was also reported for inclusive charged hadron spectra, π , K, p, K_S^0 , Λ , Ξ , and Ω in pp collisions at LHC energies [20, 22, 34, 67], where different models with multi-parton interactions were shown to describe these effects.

3.2 Integrated particle yield and mean transverse momentum

The p_T -integrated yields and mean transverse momentum are extracted from transverse momentum spectra in the measured range and using the fit function in the unmeasured region. The ϕ yield is extrapolated in the unmeasured region ($p_T < 0.4$ GeV/c) by fitting a Lévy-Tsallis functions [68] to the measured p_T spectra in all multiplicity classes. The difference in the yield contribution at low p_T due to different fitting functions (i.e exponential, Boltzmann, m_T -exponential, Bose-Einstein and Boltzmann-Gibbs Blast-Wave function in Ref. [45]) from the Lévy-Tsallis function is included in the systematic uncertainties. The low- p_T extrapolation accounts for 8.9% (14.1%) of the total yield in the 0–5% (80–100%) multiplicity class. The K^{*0} spectra are measured from $p_T = 0$, so low- p_T extrapolation is not needed. The contribution of the extrapolated fraction of the yield is negligible for $p_T > 20$ GeV/c (16 GeV/c) for

Table 3: The values of dN/dy and $\langle p_T \rangle$ are presented for different multiplicity classes in p–Pb collisions at $\sqrt{s_{NN}} = 8.16$ TeV. In each entry, the first uncertainty is statistical and the second is systematic. The value given in the parentheses corresponds to uncorrelated part of the systematic uncertainty. The fraction of total yield obtained by extrapolation (“extr.”) are also reported.

		K^{*0}	
Multiplicity (%)	extr.	dN/dy	$\langle p_T \rangle$ (GeV/c)
0–5	-	$0.913 \pm 0.030 \pm 0.086$ (0.047)	$1.509 \pm 0.033 \pm 0.028$ (0.018)
5–10	-	$0.783 \pm 0.025 \pm 0.074$ (0.050)	$1.461 \pm 0.029 \pm 0.030$ (0.021)
10–20	-	$0.644 \pm 0.015 \pm 0.060$ (0.047)	$1.460 \pm 0.021 \pm 0.028$ (0.020)
20–40	-	$0.489 \pm 0.009 \pm 0.045$ (0.028)	$1.407 \pm 0.016 \pm 0.025$ (0.017)
40–60	-	$0.344 \pm 0.006 \pm 0.032$ (0.018)	$1.301 \pm 0.014 \pm 0.025$ (0.014)
60–80	-	$0.220 \pm 0.004 \pm 0.020$ (0.016)	$1.176 \pm 0.012 \pm 0.026$ (0.020)
80–100	-	$0.092 \pm 0.002 \pm 0.008$ (0.006)	$0.950 \pm 0.011 \pm 0.026$ (0.018)
NSD	-	$0.396 \pm 0.004 \pm 0.037$	$1.335 \pm 0.008 \pm 0.027$
		ϕ	
Multiplicity (%)	extr.	dN/dy	$\langle p_T \rangle$ (GeV/c)
0–5	0.089	$0.455 \pm 0.008 \pm 0.041$ (0.026)	$1.496 \pm 0.015 \pm 0.022$ (0.021)
5–10	0.088	$0.356 \pm 0.007 \pm 0.033$ (0.028)	$1.482 \pm 0.017 \pm 0.022$ (0.021)
10–20	0.093	$0.292 \pm 0.004 \pm 0.028$ (0.018)	$1.468 \pm 0.013 \pm 0.021$ (0.016)
20–40	0.101	$0.217 \pm 0.003 \pm 0.020$ (0.008)	$1.409 \pm 0.011 \pm 0.025$ (0.010)
40–60	0.104	$0.146 \pm 0.002 \pm 0.014$ (0.007)	$1.342 \pm 0.011 \pm 0.029$ (0.021)
60–80	0.122	$0.084 \pm 0.001 \pm 0.008$ (0.004)	$1.249 \pm 0.013 \pm 0.025$ (0.020)
80–100	0.141	$0.0313 \pm 0.0008 \pm 0.003$ (0.002)	$1.097 \pm 0.016 \pm 0.029$ (0.008)
NSD	0.103	$0.161 \pm 0.002 \pm 0.015$	$1.393 \pm 0.008 \pm 0.024$

K^{*0} (ϕ). The values of dN/dy and $\langle p_T \rangle$ of K^{*0} and ϕ for various multiplicity classes are summarized in the Table 3. The multiplicity-scaled integrated yields ($dN/dy/\langle dN_{ch}/d\eta \rangle_{|\eta|<0.5}$) for K^{*0} and ϕ are shown in the upper panels of Fig. 5 as a function of $\langle dN_{ch}/d\eta \rangle_{|\eta|<0.5}$. These results are compared with other ALICE measurements in pp collisions at $\sqrt{s} = 7$ and 13 TeV [20, 22], in p–Pb collisions at $\sqrt{s_{NN}} = 5.02$ TeV [23], and in Pb–Pb collisions at $\sqrt{s_{NN}} = 2.76$ and 5.02 TeV [15, 18, 19]. The scaled integrated yields evolve smoothly as a function of multiplicity from pp, p–Pb to Pb–Pb collisions. For similar $\langle dN_{ch}/d\eta \rangle_{|\eta|<0.5}$, these values are consistent within uncertainties for different colliding systems and at various LHC energies. This indicates that event multiplicity drives the resonance production, irrespective of the colliding systems and energies [20, 22, 23].

The scaled integrated yields of ϕ show a slight increase with multiplicity from pp collisions to mid-central Pb–Pb collisions. The total increase is 12% with a 1.5σ significance between the lowest multiplicity bin and the highest multiplicity bin in p–Pb collisions at $\sqrt{s_{NN}} = 8.16$ TeV. Similarly scaled integrated yields of K^{*0} show a slight decrease with multiplicity for all three collision systems and the total decrease is 12% with a 1.8σ significance for p–Pb collisions at $\sqrt{s_{NN}} = 8.16$ TeV. The significance is calculated using statistical and multiplicity uncorrelated systematic uncertainties, added in quadrature. The integrated yield ratios of resonances relative to those of longer lived particles, π , K and p are computed to study their production mechanism. The K^{*0}/K (ϕ/π) ratio measured in p–Pb collisions at $\sqrt{s_{NN}} = 5.02$ TeV [23] shows a decreasing (increasing) trend going from the lowest multiplicity to the highest multiplicity bin with a significance of 2.6σ (1.5σ) which is discussed in the context of a hint of a re-scattering (strangeness enhancement) effect. Future measurements of π and K yields in p–Pb collisions at $\sqrt{s_{NN}} = 8.16$ TeV will be useful to study these effects at higher centre-of-mass energy and up to larger multiplicity. The model comparison with the p–Pb data shows that EPOS-LHC describes the scaled integrated yields for both K^{*0} and ϕ whereas HIJING overestimates the data for all multiplicities. The DPMJET model describes the scaled integrated yield of ϕ at higher multiplicities but overestimates the K^{*0} at all multiplicities. The $\langle p_T \rangle$ exhibits an increasing trend as a function of $\langle dN_{ch}/d\eta \rangle_{|\eta|<0.5}$ for K^{*0} and ϕ in various colliding systems and energies as shown in the bottom panels of Fig 5. The increase in $\langle p_T \rangle$

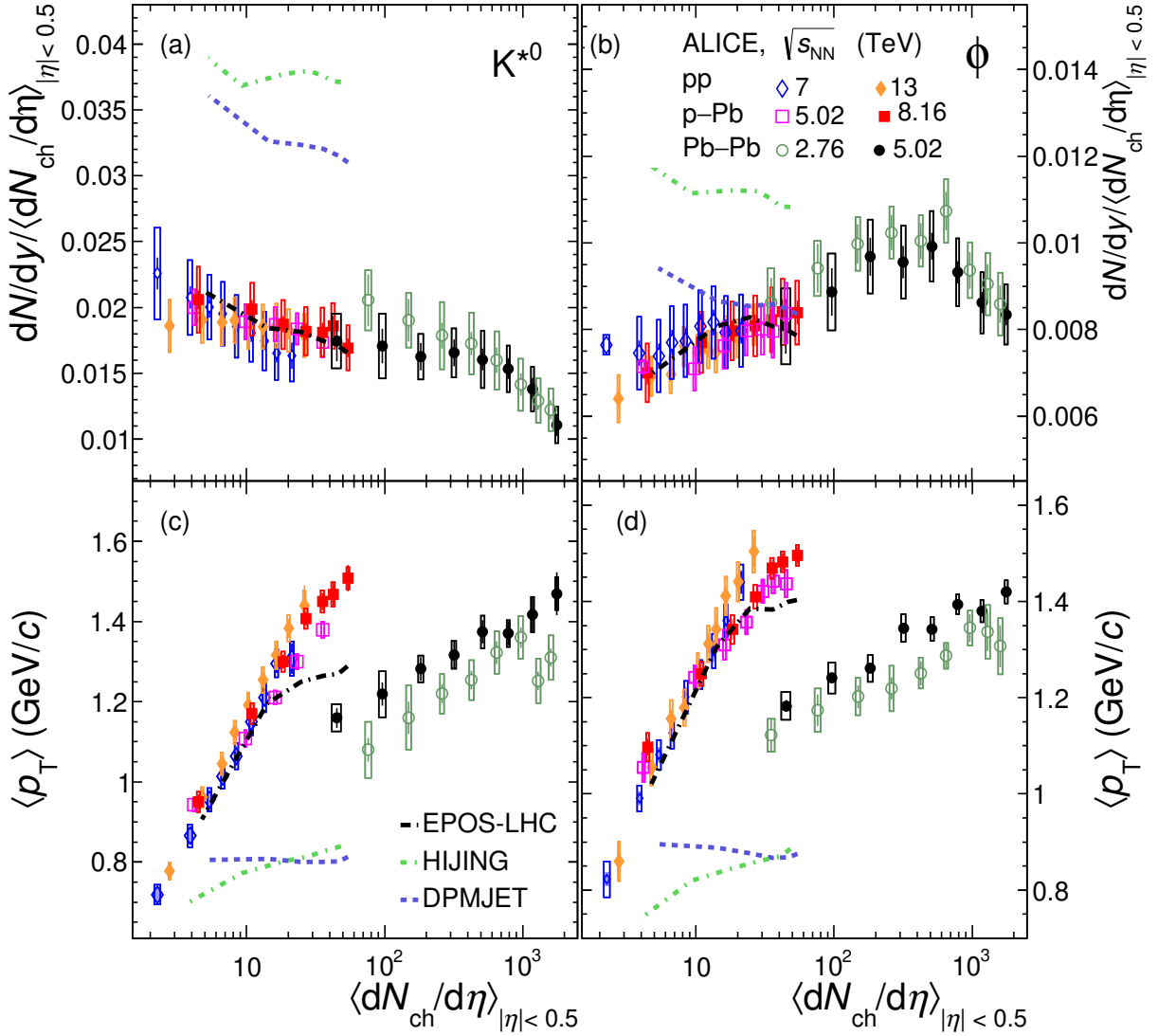


Figure 5: The multiplicity-scaled integrated yield ($dN/dy/\langle dN_{ch}/d\eta \rangle_{|\eta| < 0.5}$) (upper panels) and mean transverse momentum ($\langle p_T \rangle$) (bottom panels) for K^{*0} (left panels) and ϕ (right panels) as a function of $\langle dN_{ch}/d\eta \rangle_{|\eta| < 0.5}$ measured in the ALICE central barrel in pp collisions at $\sqrt{s} = 7, 13$ TeV, in p–Pb collisions at $\sqrt{s_{NN}} = 5.02, 8.16$ TeV and Pb–Pb collisions at $\sqrt{s_{NN}} = 2.76, 5.02$ TeV. Measurements are compared with the predictions from EPOS-LHC [31, 61], DPMJET [32] and HIJING [33] for p–Pb collisions at $\sqrt{s_{NN}} = 8.16$ TeV. Statistical uncertainties are represented as bars, boxes indicate total systematic uncertainties.

is faster for pp and p–Pb than Pb–Pb and for a common multiplicity coverage the values of $\langle p_T \rangle$ in pp and p–Pb are larger than Pb–Pb. At similar multiplicity ($\langle dN_{ch}/d\eta \rangle_{|\eta| < 0.5} \sim 40$), the difference in $\langle p_T \rangle$ values among Pb–Pb, p–Pb and pp collisions indicate that the geometry and dynamics of the collision systems are different, while the scaled integrated yields of K^{*0} and ϕ are similar for all colliding systems and energies.

Similar studies are reported in Refs. [23, 69], where the moderate increase of $\langle p_T \rangle$ in Pb–Pb collisions was related to collective flow. The strong increase of $\langle p_T \rangle$ with $\langle dN_{ch}/d\eta \rangle_{|\eta| < 0.5}$ in small collision systems can be further investigated by systematic studies of $\langle p_T \rangle$ from different models in pp and p–Pb

collisions that incorporate processes like color reconnection, between strings produced in multi-parton interactions, different string fragmentation processes and the core-corona mechanism. It was observed in Ref. [22] that the PYTHIA8 model with color reconnection, which introduces a flow-like effect, and the EPOS-LHC model, which uses parameterized flow, are able to reproduce the increasing trend of $\langle p_T \rangle$ as a function of multiplicity for K^{*0} and ϕ in pp collisions at $\sqrt{s} = 13$ TeV. The p–Pb measurements are important, as in Ref. [69] it is shown that the $\langle p_T \rangle$ of charged hadrons as a function of multiplicity shows a similar behavior as in pp collisions at low multiplicity whereas it seems to approach a similar but less prominent trend of saturation as in Pb–Pb collisions at high multiplicity.

The model comparison with p–Pb data shows that EPOS-LHC describes the increasing trend of $\langle p_T \rangle$ with multiplicity for both K^{*0} and ϕ , and it gives a better agreement for ϕ to high multiplicity values. DPMJET and HIJING models fail to describe the observed trend in $\langle p_T \rangle$ for both K^{*0} and ϕ and underpredict the data for all multiplicities.

3.3 x_T scaling

Particle invariant production cross sections are known to follow a scaling in the measurement of the transverse momentum spectrum for different collision energies at high p_T using the scaling variable $x_T = 2p_T / \sqrt{s}$ [39, 40]. The x_T scaling was tested in pp collisions for identified hadrons in STAR [44], ALICE [45] and for (non-identified) charged particles in CMS [46]. In this paper, the validity of empirical x_T scaling is tested using the K^{*0} and ϕ measurements in p–Pb collisions at $\sqrt{s_{NN}} = 8.16$ TeV reported here and those obtained at $\sqrt{s_{NN}} = 5.02$ TeV [23]. The invariant cross sections are determined from the measured invariant yield as $Ed^3\sigma/dp^3 = \sigma_{\text{inel}} \times Ed^3N/dp^3$, where $\sigma_{\text{inel}} = (72.5 \pm 0.5)$ mb and (67.6 ± 0.6) mb is the inelastic cross section in pp collisions at $\sqrt{s} = 8.16$ TeV and 5.02 TeV, respectively [70].

At fixed x_T , the invariant cross section $Ed^3\sigma/dp^3$ scales as p_T^{-n} , where the exponent of scaling n depends on x_T and $\sqrt{s_{NN}}$, and is calculated using the following equation

$$n(x_T, \sqrt{s_{NN1}}, \sqrt{s_{NN2}}) = \frac{\ln(\sigma^{\text{inv}}(x_T, \sqrt{s_{NN2}}) / \sigma^{\text{inv}}(x_T, \sqrt{s_{NN1}}))}{\ln(\sqrt{s_{NN1}} / \sqrt{s_{NN2}})}, \quad (1)$$

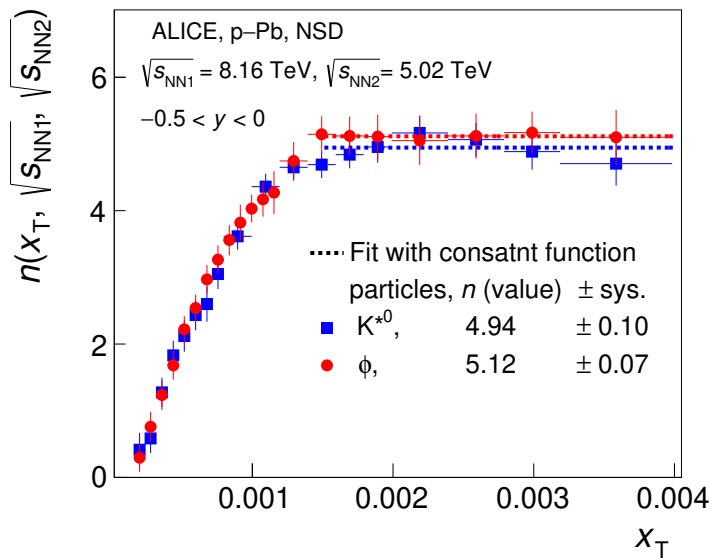


Figure 6: The values of n as a function of x_T for K^{*0} and ϕ in p–Pb collisions.

where $x_T = 2p_T/\sqrt{s_{NN}}$. The distributions of n values as a function of x_T for K^{*0} and ϕ are shown in Fig. 6. In the low x_T region, where the particle production is dominated by soft processes, the values of n are found to increase with x_T whereas the n values seem to saturate at high x_T . The n values are obtained by fitting the $n(x_T, \sqrt{s_{NN}})$ distribution by a constant function in the x_T range $1.3 \times 10^{-3} < x_T < 4 \times 10^{-3}$ for both K^{*0} and ϕ . The x_T spectra for both particles are scaled by the corresponding $(\sqrt{s_{NN}}/\text{GeV})^n$. The best scaling is obtained in the quoted fitting range with an exponent of $n = 4.94 \pm 0.10$ (sys.) for K^{*0} and $n = 5.12 \pm 0.07$ (sys.) for ϕ . The systematic uncertainties on the exponent n are calculated by changing the fit range in $n(x_T, \sqrt{s_{NN}})$ vs. x_T distribution. The maximum deviation of n value with respect to the default one is taken as systematic uncertainties. The n values for K^{*0} and ϕ are consistent within the uncertainties, which suggests that the ratios of particle spectra attain similar values in p–Pb collisions at LHC energies. The x_T -scaled spectra for K^{*0} (left panel) and ϕ (right panel) in p–Pb collisions at $\sqrt{s_{NN}} = 5.02$ and 8.16 TeV are shown in Fig. 7.

These measurements suggest that the K^{*0} and ϕ yields in p–Pb collisions at LHC energies follow x_T scaling for $x_T \gtrsim 10^{-3}$. Similar studies were performed in pp collisions at LHC energies for identified hadrons (π^\pm , K^\pm , p (\bar{p}) and K^{*0}) with ALICE [45] and for charged hadrons with CMS [46]. The n values obtained in pp collisions for all hadron species except the proton are comparable to those reported here for K^{*0} and ϕ in p–Pb collisions. In Ref. [45], the proton takes a larger value of the exponent n , which was discussed in the context of the decrease of the baryon-to-meson ratio with increasing p_T in contrast to the nearly constant behavior of meson-to-meson ratios. The n value obtained at LHC energies is also observed to be lower than at RHIC energies, which suggests an increasing contribution of hard processes at higher centre-of-mass energies.

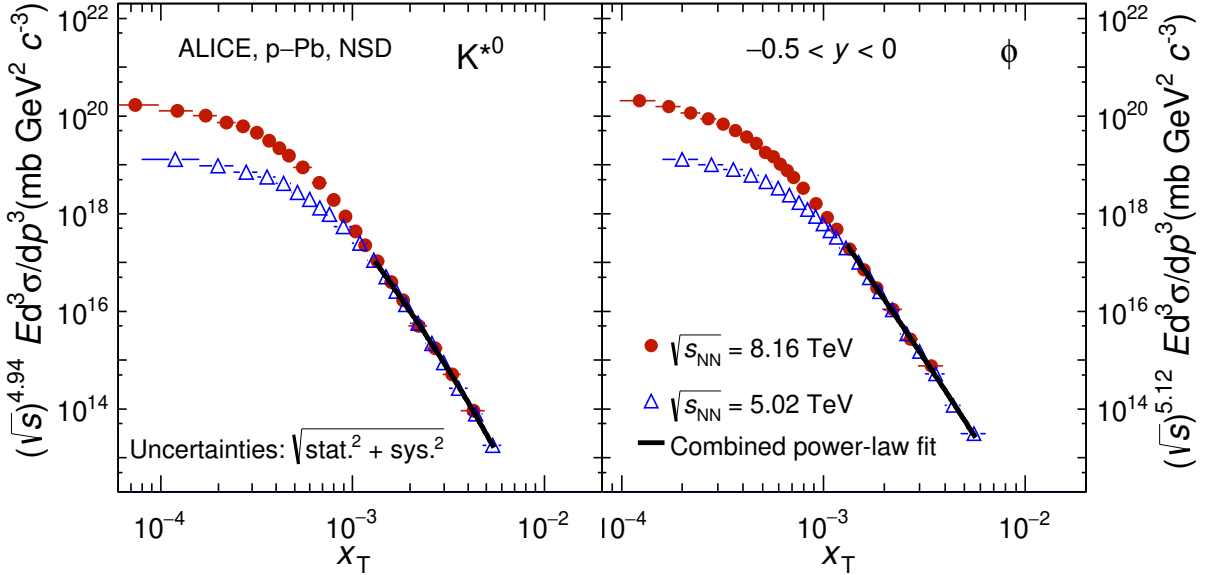


Figure 7: Scaled invariant yield of K^{*0} and ϕ as a function of $x_T = 2p_T/\sqrt{s_{NN}}$ in p–Pb collisions at different energies $\sqrt{s_{NN}} = 5.02$ and 8.16 TeV.

A combined fit to the scaled differential cross sections of K^{*0} and ϕ is performed with a power-law function of the form $a \times x_T^b \times (1+x_T)^c$ to verify the quality of the scaling behaviour. Here, a , b , and c are free parameters. The fitting is done in the region above $x_T \gtrsim 1.3 \times 10^{-3}$ (shown as black curve in Fig. 7), where the x_T scaling is observed. The χ^2/ndf value for K^{*0} (ϕ) is 0.16 (0.6), which confirms the good

quality of the fit. In the fitting region, the measurements agree with the combined power law fits within $\approx 20\%$ for both K^{*0} and ϕ . The measurements at $\sqrt{s_{NN}} = 8.16$ TeV are consistent, over the accessible x_T range $1.3 \times 10^{-3} < x_T < 3 \times 10^{-3}$, with empirical x_T scaling and with measurements from p–Pb collisions at $\sqrt{s_{NN}} = 5.02$ TeV. This further helps understanding and distinguishing the contributions of the soft and hard processes to particle production.

3.4 Nuclear modification factor (R_{pPb})

In order to understand the nuclear effects, the nuclear modification factor (R_{pPb}) is an important observable in p–Pb collisions. It is calculated as :

$$R_{pPb}(p_T) = \frac{d^2N_{pPb}/dp_T dy}{\langle T_{pPb} \rangle d^2\sigma_{pp}^{INEL}/dp_T dy}, \quad (2)$$

where $d^2N_{pPb}/dp_T dy$ is the yield in p–Pb collisions and $d^2\sigma_{pp}^{INEL}/dp_T dy$ is the invariant cross section in inelastic pp collisions. $\langle T_{pPb} \rangle = \langle N_{coll} \rangle / \sigma^{INEL}$ is the average nuclear overlap function, which accounts for the nuclear collision geometry as obtained from a Glauber model [70]. If the nuclear modification factor is unity, the yield in nuclear collisions is the same as from an incoherent superposition of nucleon–nucleon collisions.

In the absence of K^{*0} and ϕ measurements in pp collisions at $\sqrt{s} = 8.16$ TeV, the reference p_T spectra are obtained from the distributions measured in pp collisions at $\sqrt{s} = 8$ TeV [21] scaled by the ratio between the p_T spectra at the two energies as obtained from PYTHIA 8.230 [71]. For the systematic study the reference pp spectra are also obtained using the measured p_T spectrum at $\sqrt{s} = 7$ TeV [16]. The total systematic uncertainty of the pp reference spectrum is then calculated as the quadrature sum of the systematic uncertainties of the measured p_T spectrum at $\sqrt{s} = 8$ TeV and the difference of the reference spectra obtained using the measured p_T spectra at $\sqrt{s} = 7$ and 8 TeV. The systematic uncertainties of the reference p_T spectra of K^{*0} (ϕ) are 11.5% (7.3%) for the low p_T (< 4 GeV/ c) and 15.5% (7.4%) for the high p_T (> 4 GeV/ c) [26]. The systematic and statistical uncertainties of R_{pPb} are calculated as the quadrature sum of respective uncertainties of the p_T spectra in p–Pb and pp collisions. The value of the nucleon–nucleon inelastic cross section for the reference spectra at $\sqrt{s} = 8.16$ TeV is (72.5 ± 0.5) mb, taken from Ref. [70].

The R_{pPb} measurements of K^{*0} , ϕ and multi-strange baryon (Ξ and Ω) in p–Pb collisions at $\sqrt{s_{NN}} = 5.02$ TeV are also reported here. The R_{pPb} of K^{*0} and ϕ at $\sqrt{s_{NN}} = 5.02$ TeV are calculated from the measured p_T spectra in pp and p–Pb collisions published in Refs. [18, 19, 23]. The p_T spectra measurements of multi-strange baryon (Ξ and Ω) production in p–Pb collisions are reported in Ref. [27]. Due to the unavailability of multi-strange baryon measurements in pp collisions at $\sqrt{s} = 5.02$ TeV, reference p_T spectra are calculated by interpolating the measurements at $\sqrt{s} = 2.76$ [72] and 7 TeV [73], in each p_T interval, assuming a power law dependence as a function of \sqrt{s} . The systematic uncertainties of the reference p_T spectra are taken as the maximum relative systematic uncertainty of the measured p_T spectra at $\sqrt{s} = 2.76$ and 7 TeV. This approach is similar to the one as described in Ref. [26] to obtain reference p_T spectra for π^\pm , K^\pm and $p(\bar{p})$ in pp collisions at $\sqrt{s} = 5.02$ TeV. Figure 8 shows the nuclear modification factor of K^{*0} (left panel) and ϕ (right panel) as a function of p_T in p–Pb collisions at $\sqrt{s_{NN}} = 5.02$ and 8.16 TeV. At intermediate p_T (2–8 GeV/ c), there is a hint of increase in R_{pPb} , above unity which is more pronounced for K^{*0} than for ϕ . The measurements are consistent with each other within uncertainties. No significant energy dependence of R_{pPb} is observed for resonances in p–Pb collisions at the LHC energies.

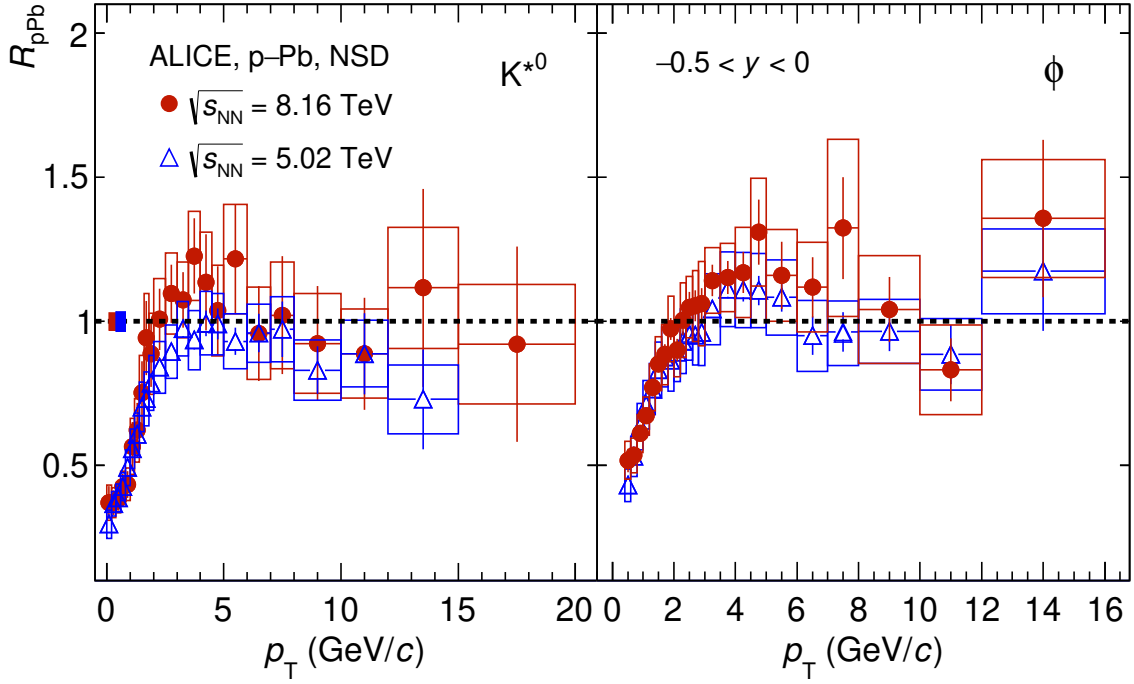


Figure 8: Nuclear modification factor of K^{*0} and ϕ as a function of p_T in p-Pb collisions at different energies $\sqrt{s_{NN}} = 5.02$ and 8.16 TeV. The statistical and systematic uncertainties are represented by vertical bars and boxes, respectively. The normalization uncertainties are shown in each panel as boxes around $R_{pPb} = 1$ near $p_T = 0$ GeV/c.

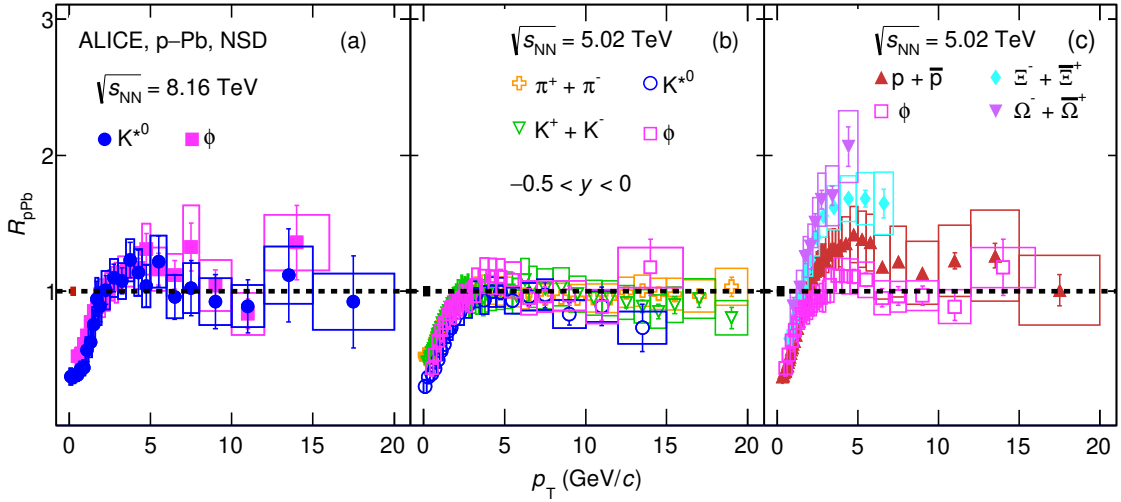


Figure 9: The nuclear modification factor R_{pPb} as a function of transverse momentum p_T for different particle species in p-Pb collisions at $\sqrt{s_{NN}} = 5.02$ and 8.16 TeV. For comparison the results for π , K, and p [26] are also shown. The statistical and systematic uncertainties are represented by vertical bars and boxes, respectively. The normalization uncertainties are shown in each panel as boxes around $R_{pPb} = 1$ near $p_T = 0$ GeV/c.

Figure 9 shows the particle species dependence of the nuclear modification factors in p-Pb collisions at

$\sqrt{s_{\text{NN}}} = 5.02$ and 8.16 TeV. Panels (a) and (b) show R_{pPb} of K^{*0} and ϕ at $\sqrt{s_{\text{NN}}} = 8.16$ and 5.02 TeV, respectively. Previous measurements of π and K mesons at $\sqrt{s_{\text{NN}}} = 5.02$ TeV [26] are also shown in panel (b). Panel (c) shows the R_{pPb} of multi-strange baryons (Ξ , Ω) at $\sqrt{s_{\text{NN}}} = 5.02$ TeV. To study the mass dependence of baryons and to compare baryons and mesons, the R_{pPb} of protons taken from [26] and that of ϕ mesons are also shown in panel (c). At low p_{T} (< 2 GeV/ c), the R_{pPb} is less than unity for all hadrons. The measurements of K^{*0} and ϕ at $\sqrt{s_{\text{NN}}} = 5.02$ and 8.16 TeV are consistent with each other within uncertainties, no flavor dependence in R_{pPb} is observed. At intermediate p_{T} (2 – 8 GeV/ c), the R_{pPb} of baryons shows a Cronin-like enhancement above unity [49]. The R_{pPb} shows a mass ordering and larger values are observed for the baryons with higher masses. A similar mass ordering for baryons in this p_{T} region is also reported by CMS in Ref. [48] and the results are consistent with a hydrodynamical expectation of the radial flow [31]. It is also observed that the R_{pPb} of ϕ meson is smaller than that of the proton in spite of their similar masses, which may indicate baryon-meson ordering. Therefore, along with the presence of a strong radial flow component, there are other effects like different production mechanism for baryons and mesons which affect the R_{pPb} in this p_{T} region. Similar behavior is also observed in Pb–Pb collisions in this p_{T} region [36]. At high p_{T} (> 8 GeV/ c), the R_{pPb} values of all particles are consistent with unity within the uncertainties in p–Pb collisions at $\sqrt{s_{\text{NN}}} = 5.02$ and 8.16 TeV which suggests that there is no modification in R_{pPb} due to cold nuclear matter effects for different particle species. Similar findings are also reported for π^0 meson with p_{T} up to 200 GeV/ c in p–Pb collisions at $\sqrt{s_{\text{NN}}} = 8.16$ TeV [74], for charged hadrons in p–Pb collisions at $\sqrt{s_{\text{NN}}} = 5.02$ TeV by ALICE [26, 47], and for strange hadrons by CMS in p–Pb collisions at $\sqrt{s_{\text{NN}}} = 5.02$ TeV [48] and by STAR in d–Au collisions at $\sqrt{s_{\text{NN}}} = 200$ GeV [25].

4 Summary

The production of K^{*0} and ϕ mesons as a function of p_{T} has been measured in the rapidity interval $-0.5 < y < 0$ for various multiplicity classes in p–Pb collisions at $\sqrt{s_{\text{NN}}} = 8.16$ TeV with the ALICE detector. The EPOS-LHC model describes the NSD p_{T} distribution while the DPMJET and HIJING models largely overestimate the distribution at low p_{T} . A significant evolution of spectral shapes with multiplicity is observed for $p_{\text{T}} < 4$ GeV/ c , with a pattern similar to that of Pb–Pb collisions, which can be attributed to the collective radial expansion of the system. The spectral shapes are similar for all multiplicity classes at high p_{T} . The scaled p_{T} -integrated yields ($dN/dy/\langle dN_{\text{ch}}/d\eta \rangle_{|\eta|<0.5}$) as a function of multiplicity show a smooth evolution from small systems, pp and p–Pb, to Pb–Pb, and the values are similar for a given multiplicity, irrespective of the colliding systems and energies, suggesting that the hadrochemistry of the particle production is mainly driven by the event multiplicity. The $\langle p_{\text{T}} \rangle$ values of K^{*0} and ϕ increase as a function of multiplicity and follow a different trend in p–Pb and pp than Pb–Pb collisions. The EPOS-LHC model which includes parameterized flow gives a good quantitative description of the scaled p_{T} -integrated yields and describes qualitatively the increase in $\langle p_{\text{T}} \rangle$ values with multiplicity for both K^{*0} and ϕ . An empirical x_{T} scaling for K^{*0} and ϕ holds (within roughly 20%) in the hard scattering region of the particle production. The obtained value of the exponent ($n \sim 5$) is lower than at RHIC energies which suggests an increasing contribution of hard scattering processes at higher $\sqrt{s_{\text{NN}}}$. Furthermore, the value of the exponent n in p–Pb collisions is compatible with those in pp collisions for π^{\pm} , K^{\pm} and K^{*0} suggesting that the high- p_{T} particle production mechanism is similar in both collision systems. No significant energy dependence in R_{pPb} is observed for K^{*0} and ϕ in p–Pb collisions at $\sqrt{s_{\text{NN}}} = 5.02$ and 8.16 TeV. At intermediate p_{T} ($2 < p_{\text{T}} < 8$ GeV/ c), R_{pPb} values for multi-strange baryon (Ξ and Ω) and the protons in p–Pb collisions at $\sqrt{s_{\text{NN}}} = 5.02$ TeV show a Cronin-like enhancement and the values are found to be significantly larger than those for π^{\pm} , K^{\pm} , K^{*0} and ϕ . The R_{pPb} values are consistent with unity within the uncertainties for all species at $p_{\text{T}} > 8$ GeV/ c , which further confirms the absence of cold-nuclear matter effects in this p_{T} range. Future measurements of light flavor hadron (π^{\pm} , K^{\pm} , $p(\bar{p})$ etc.) yields up to high p_{T} in p–Pb collisions at $\sqrt{s_{\text{NN}}} = 8.16$ TeV are required for a comprehensive study of nuclear modification factor and x_{T} scaling.

Acknowledgements

The ALICE Collaboration would like to thank all its engineers and technicians for their invaluable contributions to the construction of the experiment and the CERN accelerator teams for the outstanding performance of the LHC complex. The ALICE Collaboration gratefully acknowledges the resources and support provided by all Grid centres and the Worldwide LHC Computing Grid (WLCG) collaboration. The ALICE Collaboration acknowledges the following funding agencies for their support in building and running the ALICE detector: A. I. Alikhanyan National Science Laboratory (Yerevan Physics Institute) Foundation (ANSL), State Committee of Science and World Federation of Scientists (WFS), Armenia; Austrian Academy of Sciences, Austrian Science Fund (FWF): [M 2467-N36] and Nationalstiftung für Forschung, Technologie und Entwicklung, Austria; Ministry of Communications and High Technologies, National Nuclear Research Center, Azerbaijan; Conselho Nacional de Desenvolvimento Científico e Tecnológico (CNPq), Financiadora de Estudos e Projetos (Finep), Fundação de Amparo à Pesquisa do Estado de São Paulo (FAPESP) and Universidade Federal do Rio Grande do Sul (UFRGS), Brazil; Ministry of Education of China (MOEC), Ministry of Science & Technology of China (MSTC) and National Natural Science Foundation of China (NSFC), China; Ministry of Science and Education and Croatian Science Foundation, Croatia; Centro de Aplicaciones Tecnológicas y Desarrollo Nuclear (CEADEN), Cubaenergía, Cuba; Ministry of Education, Youth and Sports of the Czech Republic, Czech Republic; The Danish Council for Independent Research | Natural Sciences, the VILLUM FONDEN and Danish National Research Foundation (DNRF), Denmark; Helsinki Institute of Physics (HIP), Finland; Commissariat à l’Energie Atomique (CEA) and Institut National de Physique Nucléaire et de Physique des Particules (IN2P3) and Centre National de la Recherche Scientifique (CNRS), France; Bundesministerium für Bildung und Forschung (BMBF) and GSI Helmholtzzentrum für Schwerionenforschung GmbH, Germany; General Secretariat for Research and Technology, Ministry of Education, Research and Religions, Greece; National Research, Development and Innovation Office, Hungary; Department of Atomic Energy Government of India (DAE), Department of Science and Technology, Government of India (DST), University Grants Commission, Government of India (UGC) and Council of Scientific and Industrial Research (CSIR), India; Indonesian Institute of Science, Indonesia; Istituto Nazionale di Fisica Nucleare (INFN), Italy; Japanese Ministry of Education, Culture, Sports, Science and Technology (MEXT), Japan Society for the Promotion of Science (JSPS) KAKENHI and Japanese Ministry of Education, Culture, Sports, Science and Technology (MEXT) of Applied Science (IIST), Japan; Consejo Nacional de Ciencia (CONACYT) y Tecnología, through Fondo de Cooperación Internacional en Ciencia y Tecnología (FONCICYT) and Dirección General de Asuntos del Personal Académico (DGAPA), Mexico; Nederlandse Organisatie voor Wetenschappelijk Onderzoek (NWO), Netherlands; The Research Council of Norway, Norway; Commission on Science and Technology for Sustainable Development in the South (COMSATS), Pakistan; Pontificia Universidad Católica del Perú, Peru; Ministry of Education and Science, National Science Centre and WUT ID-UB, Poland; Korea Institute of Science and Technology Information and National Research Foundation of Korea (NRF), Republic of Korea; Ministry of Education and Scientific Research, Institute of Atomic Physics and Ministry of Research and Innovation and Institute of Atomic Physics, Romania; Joint Institute for Nuclear Research (JINR), Ministry of Education and Science of the Russian Federation, National Research Centre Kurchatov Institute, Russian Science Foundation and Russian Foundation for Basic Research, Russia; Ministry of Education, Science, Research and Sport of the Slovak Republic, Slovakia; National Research Foundation of South Africa, South Africa; Swedish Research Council (VR) and Knut & Alice Wallenberg Foundation (KAW), Sweden; European Organization for Nuclear Research, Switzerland; Suranaree University of Technology (SUT), National Science and Technology Development Agency (NSDTA) and Office of the Higher Education Commission under NRU project of Thailand, Thailand; Turkish Energy, Nuclear and Mineral Research Agency (TENMAK), Turkey; National Academy of Sciences of Ukraine, Ukraine; Science and Technology Facilities Council (STFC), United Kingdom;

National Science Foundation of the United States of America (NSF) and United States Department of Energy, Office of Nuclear Physics (DOE NP), United States of America.

References

- [1] P. Braun-Munzinger, V. Koch, T. Schäfer, and J. Stachel, “Properties of hot and dense matter from relativistic heavy ion collisions”, *Phys. Rept.* **621** (2016) 76–126, arXiv:1510.00442 [nucl-th].
- [2] STAR Collaboration, J. Adams *et al.*, “Experimental and theoretical challenges in the search for the quark gluon plasma: The STAR Collaboration’s critical assessment of the evidence from RHIC collisions”, *Nucl. Phys.* **A757** (2005) 102–183, arXiv:nucl-ex/0501009 [nucl-ex].
- [3] ALICE Collaboration, J. Schukraft, “Heavy Ion physics with the ALICE experiment at the CERN LHC”, *Phil. Trans. Roy. Soc. Lond. A* **370** (2012) 917–932, arXiv:1109.4291 [hep-ex].
- [4] STAR Collaboration, M. M. Aggarwal *et al.*, “ K^{*0} production in Cu+Cu and Au+Au collisions at $\sqrt{s_{NN}} = 62.4$ GeV and 200 GeV”, *Phys. Rev.* **C84** (2011) 034909, arXiv:1006.1961 [nucl-ex].
- [5] STAR Collaboration, J. Adams *et al.*, “ $K^*(892)^0$ resonance production in Au+Au and p+p collisions at $\sqrt{s_{NN}} = 200$ GeV at STAR”, *Phys. Rev.* **C71** (2005) 064902, arXiv:nucl-ex/0412019 [nucl-ex].
- [6] STAR Collaboration, C. Adler *et al.*, “ $K^*(892)^0$ production in relativistic heavy ion collisions at $\sqrt{s_{NN}} = 130$ GeV”, *Phys. Rev.* **C66** (2002) 061901, arXiv:nucl-ex/0205015 [nucl-ex].
- [7] NA49 Collaboration, T. Anticic *et al.*, “ $K^*(892)^0$ and $\bar{K}^*(892)^0$ production in central Pb+Pb, Si+Si, C+C and inelastic p+p collisions at 158A GeV”, *Phys. Rev.* **C84** (2011) 064909, arXiv:1105.3109 [nucl-ex].
- [8] STAR Collaboration, B. I. Abelev *et al.*, “Energy and system size dependence of ϕ meson production in Cu+Cu and Au+Au collisions”, *Phys. Lett.* **B673** (2009) 183–191, arXiv:0810.4979 [nucl-ex].
- [9] STAR Collaboration, B. I. Abelev *et al.*, “Measurements of ϕ meson production in relativistic heavy-ion collisions at RHIC”, *Phys. Rev.* **C79** (2009) 064903, arXiv:0809.4737 [nucl-ex].
- [10] STAR Collaboration, L. Adamczyk *et al.*, “Probing parton dynamics of QCD matter with Ω and ϕ production”, *Phys. Rev.* **C93** no. 2, (2016) 021903, arXiv:1506.07605 [nucl-ex].
- [11] NA49 Collaboration, C. Alt *et al.*, “Energy dependence of ϕ meson production in central Pb+Pb collisions at $\sqrt{s_{NN}} = 6$ to 17 GeV”, *Phys. Rev.* **C78** (2008) 044907, arXiv:0806.1937 [nucl-ex].
- [12] PHENIX Collaboration, A. Adare *et al.*, “Nuclear modification factors of ϕ mesons in d +Au, Cu+Cu and Au+Au collisions at $\sqrt{s_{NN}} = 200$ GeV”, *Phys. Rev.* **C83** (2011) 024909, arXiv:1004.3532 [nucl-ex].
- [13] ALICE Collaboration, B. Abelev *et al.*, “ $K^*(892)^0$ and $\phi(1020)$ production in Pb-Pb collisions at $\sqrt{s_{NN}} = 2.76$ TeV”, *Phys. Rev.* **C91** (2015) 024609, arXiv:1404.0495 [nucl-ex].
- [14] PHENIX Collaboration, A. Adare *et al.*, “Measurement of K^{*0} in $p + p$, d +Au, and Cu+Cu collisions at $\sqrt{s_{NN}} = 200$ GeV”, *Phys. Rev.* **C90** no. 5, (2014) 054905, arXiv:1405.3628 [nucl-ex].

- [15] ALICE Collaboration, J. Adam *et al.*, “ $K^*(892)^0$ and $\phi(1020)$ meson production at high transverse momentum in pp and Pb–Pb collisions at $\sqrt{s_{NN}} = 2.76$ TeV”, *Phys. Rev.* **C95** no. 6, (2017) 064606, arXiv:1702.00555 [nucl-ex].
- [16] ALICE Collaboration, B. Abelev *et al.*, “Production of $K^*(892)^0$ and $\phi(1020)$ in pp collisions at $\sqrt{s} = 7$ TeV”, *Eur. Phys. J.* **C72** (2012) 2183, arXiv:1208.5717 [hep-ex].
- [17] ALICE Collaboration, J. Adam *et al.*, “Enhanced production of multi-strange hadrons in high-multiplicity proton-proton collisions”, *Nature Phys.* **13** (2017) 535–539, arXiv:1606.07424 [nucl-ex].
- [18] ALICE Collaboration, S. Acharya *et al.*, “Evidence of rescattering effect in Pb–Pb collisions at the LHC through production of $K^*(892)^0$ and $\phi(1020)$ mesons”, *Phys. Lett.* **B802** (2020) 135225, arXiv:1910.14419 [nucl-ex].
- [19] ALICE Collaboration, S. Acharya *et al.*, “Production of $K^*(892)^0$ and $\phi(1020)$ in pp and Pb–Pb collisions at $\sqrt{s_{NN}} = 5.02$ TeV”, arXiv:2106.13113 [nucl-ex].
- [20] ALICE Collaboration, S. Acharya *et al.*, “Multiplicity dependence of light-flavor hadron production in pp collisions at $\sqrt{s} = 7$ TeV”, *Phys. Rev.* **C99** no. 2, (2019) 024906, arXiv:1807.11321 [nucl-ex].
- [21] ALICE Collaboration, S. Acharya *et al.*, “ $K^*(892)^0$ and $\phi(1020)$ production at midrapidity in pp collisions at $\sqrt{s} = 8$ TeV”, *Phys. Rev.* **C102** no. 2, (2020) 024912, arXiv:1910.14410 [nucl-ex].
- [22] ALICE Collaboration, S. Acharya *et al.*, “Multiplicity dependence of $K^*(892)^0$ and $\phi(1020)$ production in pp collisions at $\sqrt{s} = 13$ TeV”, *Phys. Lett.* **B807** (2020) 135501, arXiv:1910.14397 [nucl-ex].
- [23] ALICE Collaboration, J. Adam *et al.*, “Production of $K^*(892)^0$ and $\phi(1020)$ in p–Pb collisions at $\sqrt{s_{NN}} = 5.02$ TeV”, *Eur. Phys. J.* **C76** no. 5, (2016) 245, arXiv:1601.07868 [nucl-ex].
- [24] ALICE Collaboration, B. Abelev *et al.*, “Transverse sphericity of primary charged particles in minimum bias proton-proton collisions at $\sqrt{s} = 0.9, 2.76$ and 7 TeV”, *Eur. Phys. J.* **C72** (2012) 2124, arXiv:1205.3963 [hep-ex].
- [25] STAR Collaboration, B. I. Abelev *et al.*, “Hadronic resonance production in d+Au collisions at $\sqrt{s_{NN}} = 200$ GeV at RHIC”, *Phys. Rev.* **C78** (2008) 044906, arXiv:0801.0450 [nucl-ex].
- [26] ALICE Collaboration, J. Adam *et al.*, “Multiplicity dependence of charged pion, kaon, and (anti)proton production at large transverse momentum in p–Pb collisions at $\sqrt{s_{NN}} = 5.02$ TeV”, *Phys. Lett.* **B760** (2016) 720–735, arXiv:1601.03658 [nucl-ex].
- [27] ALICE Collaboration, J. Adam *et al.*, “Multi-strange baryon production in p–Pb collisions at $\sqrt{s_{NN}} = 5.02$ TeV”, *Phys. Lett.* **B758** (2016) 389–401, arXiv:1512.07227 [nucl-ex].
- [28] ALICE Collaboration, S. Acharya *et al.*, “Measurement of $\Lambda(1520)$ production in pp collisions at $\sqrt{s} = 7$ TeV and p–Pb collisions at $\sqrt{s_{NN}} = 5.02$ TeV”, *Eur. Phys. J.* **C80** no. 2, (2020) 160, arXiv:1909.00486 [nucl-ex].
- [29] ALICE Collaboration, D. Adamova *et al.*, “Production of $\Sigma(1385)^\pm$ and $\Xi(1530)^0$ in p–Pb collisions at $\sqrt{s_{NN}} = 5.02$ TeV”, *Eur. Phys. J. C* **77** no. 6, (2017) 389, arXiv:1701.07797 [nucl-ex].

- [30] **ALICE** Collaboration, B. B. Abelev *et al.*, “Production of $\Sigma(1385)^\pm$ and $\Xi(1530)^0$ in proton-proton collisions at $\sqrt{s} = 7$ TeV”, *Eur. Phys. J. C* **75** no. 1, (2015) 1, arXiv:1406.3206 [nucl-ex].
- [31] T. Pierog, I. Karpenko, J. M. Katzy, E. Yatsenko, and K. Werner, “EPOS LHC: Test of collective hadronization with data measured at the CERN Large Hadron Collider”, *Phys. Rev.* **C92** no. 3, (2015) 034906, arXiv:1306.0121 [hep-ph].
- [32] S. Roesler, R. Engel, and J. Ranft, “The Monte Carlo event generator DPMJET-III”, 12, 2000. arXiv:hep-ph/0012252.
- [33] M. Gyulassy and X.-N. Wang, “HIJING 1.0: A Monte Carlo program for parton and particle production in high-energy hadronic and nuclear collisions”, *Comput. Phys. Commun.* **83** (1994) 307, arXiv:nucl-th/9502021 [nucl-th].
- [34] **ALICE** Collaboration, S. Acharya *et al.*, “Multiplicity dependence of (multi-)strange hadron production in proton-proton collisions at $\sqrt{s} = 13$ TeV”, *Eur. Phys. J.* **C80** no. 2, (2020) 167, arXiv:1908.01861 [nucl-ex].
- [35] **ALICE** Collaboration, B. Abelev *et al.*, “Centrality dependence of π , K, p production in Pb-Pb collisions at $\sqrt{s_{NN}} = 2.76$ TeV”, *Phys. Rev.* **C88** (2013) 044910, arXiv:1303.0737 [hep-ex].
- [36] **ALICE** Collaboration, S. Acharya *et al.*, “Production of charged pions, kaons, and (anti-)protons in Pb-Pb and inelastic pp collisions at $\sqrt{s_{NN}} = 5.02$ TeV”, *Phys. Rev.* **C101** no. 4, (2020) 044907, arXiv:1910.07678 [nucl-ex].
- [37] J. C. Collins, D. E. Soper, and G. F. Sterman, “Factorization of Hard Processes in QCD”, *Adv. Ser. Direct. High Energy Phys.* **5** (1989) 1–91, arXiv:hep-ph/0409313.
- [38] D. de Florian, R. Sassot, M. Epele, R. J. Hernández-Pinto, and M. Stratmann, “Parton-to-Pion Fragmentation Reloaded”, *Phys. Rev.* **D91** no. 1, (2015) 014035, arXiv:1410.6027 [hep-ph].
- [39] S. J. Brodsky, H. J. Pirner, and J. Raufeisen, “Scaling properties of high p_T inclusive hadron production”, *Phys. Lett. B* **637** (2006) 58–63, arXiv:hep-ph/0510315.
- [40] F. Arleo, S. J. Brodsky, D. S. Hwang, and A. M. Sickles, “Higher-Twist Dynamics in Large Transverse Momentum Hadron Production”, *Phys. Rev. Lett.* **105** (2010) 062002, arXiv:0911.4604 [hep-ph].
- [41] **CDF** Collaboration, T. Aaltonen *et al.*, “Measurement of Particle Production and Inclusive Differential Cross Sections in $p\bar{p}$ Collisions at $\sqrt{s} = 1.96$ TeV”, *Phys. Rev.* **D79** (2009) 112005, arXiv:0904.1098 [hep-ex]. [Erratum: *Phys. Rev.* **D82**, 119903(2010)].
- [42] **CDF** Collaboration, F. Abe *et al.*, “Transverse Momentum Distributions of Charged Particles Produced in $\bar{p}p$ Interactions at $\sqrt{s} = 630$ and 1800 GeV”, *Phys. Rev. Lett.* **61** (1988) 1819.
- [43] **UA1** Collaboration, C. Albajar *et al.*, “A Study of the General Characteristics of $p\bar{p}$ Collisions at $\sqrt{s} = 0.2$ TeV to 0.9 TeV”, *Nucl. Phys.* **B335** (1990) 261–287.
- [44] **STAR** Collaboration, J. Adams *et al.*, “Identified hadron spectra at large transverse momentum in p+p and d+Au collisions at $\sqrt{s_{NN}} = 200$ GeV”, *Phys. Lett.* **B637** (2006) 161–169, arXiv:nucl-ex/0601033 [nucl-ex].
- [45] **ALICE** Collaboration, S. Acharya *et al.*, “Production of light-flavor hadrons in pp collisions at $\sqrt{s} = 7$ and $\sqrt{s} = 13$ TeV”, *Eur. Phys. J. C* **81** no. 3, (2021) 256, arXiv:2005.11120 [nucl-ex].

- [46] **CMS** Collaboration, S. Chatrchyan *et al.*, “Charged particle transverse momentum spectra in pp collisions at $\sqrt{s} = 0.9$ and 7 TeV”, *JHEP* **08** (2011) 086, arXiv:1104.3547 [hep-ex].
- [47] **ALICE** Collaboration, S. Acharya *et al.*, “Transverse momentum spectra and nuclear modification factors of charged particles in pp , p–Pb and Pb–Pb collisions at the LHC”, *JHEP* **11** (2018) 013, arXiv:1802.09145 [nucl-ex]. [https://doi.org/10.1007/JHEP11\(2018\)013](https://doi.org/10.1007/JHEP11(2018)013).
- [48] **CMS** Collaboration, A. M. Sirunyan *et al.*, “Strange hadron production in pp and pPb collisions at $\sqrt{s_{NN}} = 5.02$ TeV”, *Phys. Rev. C* **101** no. 6, (2020) 064906, arXiv:1910.04812 [hep-ex].
- [49] Yu. V. Kovchegov, “Cronin effect and high- p_T suppression in p(d)A collisions”, *J. Phys.* **G30** (2004) S979–S982.
- [50] R. J. Fries, B. Muller, C. Nonaka, and S. A. Bass, “Hadronization in heavy ion collisions: Recombination and fragmentation of partons”, *Phys. Rev. Lett.* **90** (2003) 202303, arXiv:nucl-th/0301087 [nucl-th].
- [51] **ALICE** Collaboration, K. Aamodt *et al.*, “The ALICE experiment at the CERN LHC”, *JINST* **3** (2008) S08002.
- [52] **ALICE** Collaboration, B. Abelev *et al.*, “Performance of the ALICE Experiment at the CERN LHC”, *Int. J. Mod. Phys. A* **29** (2014) 1430044, arXiv:1402.4476 [nucl-ex].
- [53] **ALICE** Collaboration, E. Abbas *et al.*, “Performance of the ALICE VZERO system”, *JINST* **8** (2013) P10016, arXiv:1306.3130 [nucl-ex].
- [54] **ALICE** Collaboration, S. Acharya *et al.*, “Charged-particle pseudorapidity density at mid-rapidity in p–Pb collisions at $\sqrt{s_{NN}} = 8.16$ TeV”, *Eur. Phys. J. C* **79** no. 4, (2019) 307, arXiv:1812.01312 [nucl-ex].
- [55] **ALICE** Collaboration, K. Aamodt *et al.*, “Alignment of the ALICE Inner Tracking System with cosmic-ray tracks”, *JINST* **5** (2010) P03003, arXiv:1001.0502 [physics.ins-det].
- [56] J. Alme *et al.*, “The ALICE TPC, a large 3-dimensional tracking device with fast readout for ultra-high multiplicity events”, *Nucl. Instrum. Meth. A* **622** (2010) 316–367, arXiv:1001.1950 [physics.ins-det].
- [57] **ALICE** Collaboration, J. Adam *et al.*, “Measurement of pion, kaon and proton production in proton–proton collisions at $\sqrt{s} = 7$ TeV”, *Eur. Phys. J. C* **75** no. 5, (2015) 226, arXiv:1504.00024 [nucl-ex].
- [58] A. Akindinov *et al.*, “Performance of the ALICE Time-Of-Flight detector at the LHC”, *Eur. Phys. J. Plus* **128** (2013) 44.
- [59] **Particle Data Group** Collaboration, M. Tanabashi *et al.*, “Review of Particle Physics”, *Phys. Rev. D* **98** no. 3, (2018) 030001.
- [60] R. Brun, F. Bruyant, M. Maire, A. C. McPherson, and P. Zancarini, *GEANT 3: user’s guide Geant 3.10, Geant 3.11; rev. version*. CERN, Geneva, 1987. <https://cds.cern.ch/record/1119728>.
- [61] K. Werner, B. Guiot, I. Karpenko, and T. Pierog, “Analyzing radial flow features in p–Pb and p–p collisions at several TeV by studying identified-particle production with the event generator EPOS3”, *Phys. Rev. C* **89** no. 6, (2014) 064903, arXiv:1312.1233 [nucl-th].
- [62] K. Werner, I. Karpenko, M. Bleicher, and T. Pierog, “The Physics of EPOS”, *EPJ Web Conf.* **52** (2013) 05001.

- [63] H. J. Drescher, M. Hladik, S. Ostapchenko, T. Pierog, and K. Werner, “Parton-based Gribov-Regge theory”, *Phys. Rept.* **350** (2001) 93–289, arXiv:hep-ph/0007198 [hep-ph].
- [64] K. Werner, “Core-corona separation in ultrarelativistic heavy ion collisions”, *Phys. Rev. Lett.* **98** (2007) 152301, arXiv:0704.1270 [nucl-th].
- [65] T. Pierog and K. Werner, “EPOS Model and Ultra High Energy Cosmic Rays”, *Nucl. Phys. Proc. Suppl.* **196** (2009) 102–105, arXiv:0905.1198 [hep-ph].
- [66] K. Werner, I. Karpenko, T. Pierog, M. Bleicher, and K. Mikhailov, “Event-by-Event Simulation of the Three-Dimensional Hydrodynamic Evolution from Flux Tube Initial Conditions in Ultrarelativistic Heavy Ion Collisions”, *Phys. Rev. C* **82** (2010) 044904, arXiv:1004.0805 [nucl-th].
- [67] ALICE Collaboration, S. Acharya *et al.*, “Charged-particle production as a function of multiplicity and transverse sphericity in pp collisions at $\sqrt{s} = 5.02$ and 13 TeV”, *Eur. Phys. J.* **C79** no. 10, (2019) 857, arXiv:1905.07208 [nucl-ex].
- [68] C. Tsallis, “Possible Generalization of Boltzmann-Gibbs Statistics”, *J. Statist. Phys.* **52** (1988) 479–487. <https://doi.org/10.1007/BF01016429>.
- [69] ALICE Collaboration, B. Abelev *et al.*, “Multiplicity dependence of the average transverse momentum in pp, p-Pb, and Pb-Pb collisions at the LHC”, *Phys. Lett.* **B727** (2013) 371–380, arXiv:1307.1094 [nucl-ex].
- [70] C. Loizides, J. Kamin, and D. d’Enterria, “Improved Monte Carlo Glauber predictions at present and future nuclear colliders”, *Phys. Rev.* **C97** no. 5, (2018) 054910, arXiv:1710.07098 [nucl-ex]. [Erratum: Phys. Rev.C99,no.1,019901(2019)].
- [71] T. Sjöstrand, S. Ask, J. R. Christiansen, R. Corke, N. Desai, P. Ilten, S. Mrenna, S. Prestel, C. O. Rasmussen, and P. Z. Skands, “An introduction to PYTHIA 8.2”, *Comput. Phys. Commun.* **191** (2015) 159–177, arXiv:1410.3012 [hep-ph].
- [72] ALICE Collaboration, B. Abelev *et al.*, “Multi-strange baryon production at mid-rapidity in Pb–Pb collisions at $\sqrt{s_{NN}} = 2.76$ TeV”, *Phys. Lett.* **B728** (2014) 216–227, arXiv:1307.5543 [nucl-ex]. [Erratum: Phys. Lett.B734,409(2014)].
- [73] ALICE Collaboration, B. Abelev *et al.*, “Multi-strange baryon production in pp collisions at $\sqrt{s} = 7$ TeV with ALICE”, *Phys. Lett.* **B712** (2012) 309–318, arXiv:1204.0282 [nucl-ex].
- [74] ALICE Collaboration, S. Acharya *et al.*, “Nuclear modification factor of light neutral-meson spectra up to high transverse momentum in p-Pb collisions at $\sqrt{s_{NN}} = 8.16$ TeV”, arXiv:2104.03116 [nucl-ex].

A The ALICE Collaboration

S. Acharya¹⁴², D. Adamová⁹⁷, A. Adler⁷⁵, J. Adolfsson⁸², G. Aglieri Rinella³⁴, M. Agnello³⁰, N. Agrawal⁵⁴, Z. Ahammed¹⁴², S. Ahmad¹⁶, S.U. Ahn⁷⁷, I. Ahuja³⁸, Z. Akbar⁵¹, A. Akindinov⁹⁴, M. Al-Turany¹⁰⁹, S.N. Alam¹⁶, D. Aleksandrov⁹⁰, B. Alessandro⁶⁰, H.M. Alfanda⁷, R. Alfaro Molina⁷², B. Ali¹⁶, Y. Ali¹⁴, A. Alici²⁵, N. Alizadehvandchali¹²⁶, A. Alkin³⁴, J. Alme²¹, T. Alt⁶⁹, I. Altsybeev¹¹⁴, M.N. Anaam⁷, C. Andrei⁴⁸, D. Andreou⁹², A. Andronic¹⁴⁵, M. Angeletti³⁴, V. Anguelov¹⁰⁶, F. Antinori⁵⁷, P. Antonioli⁵⁴, C. Anuj¹⁶, N. Apadula⁸¹, L. Aphecetche¹¹⁶, H. Appelshäuser⁶⁹, S. Arcelli²⁵, R. Arnaldi⁶⁰, I.C. Arsene²⁰, M. Arslandok¹⁴⁷, A. Augustinus³⁴, R. Averbeck¹⁰⁹, S. Aziz⁷⁹, M.D. Azmi¹⁶, A. Badalà⁵⁶, Y.W. Baek⁴¹, X. Bai^{130,109}, R. Bailhache⁶⁹, Y. Bailung⁵⁰, R. Bala¹⁰³, A. Balbino³⁰, A. Baldisseri¹³⁹, B. Balis², D. Banerjee⁴, R. Barbera²⁶, L. Barioglio¹⁰⁷, M. Barlou⁸⁶, G.G. Barnaföldi¹⁴⁶, L.S. Barnby⁹⁶, V. Barret¹³⁶, C. Bartels¹²⁹, K. Barth³⁴, E. Bartsch⁶⁹, F. Baruffaldi²⁷, N. Bastid¹³⁶, S. Basu⁸², G. Batigne¹¹⁶, B. Batyunya⁷⁶, D. Bauri⁴⁹, J.L. Bazo Alba¹¹³, I.G. Bearden⁹¹, C. Beattie¹⁴⁷, I. Belikov¹³⁸, A.D.C. Bell Hechavarria¹⁴⁵, F. Bellini²⁵, R. Bellwied¹²⁶, S. Belokurova¹¹⁴, V. Belyaev⁹⁵, G. Bencedi^{146,70}, S. Beole²⁴, A. Bercuci⁴⁸, Y. Berdnikov¹⁰⁰, A. Berdnikova¹⁰⁶, L. Bergmann¹⁰⁶, M.G. Besoiu⁶⁸, L. Betev³⁴, P.P. Bhaduri¹⁴², A. Bhasin¹⁰³, I.R. Bhat¹⁰³, M.A. Bhat⁴, B. Bhattacharjee⁴², P. Bhattacharya²², L. Bianchi²⁴, N. Bianchi⁵², J. Bielčík³⁷, J. Bielčíková⁹⁷, J. Biernat¹¹⁹, A. Bilandzic¹⁰⁷, G. Biro¹⁴⁶, S. Biswas⁴, J.T. Blair¹²⁰, D. Blau^{90,83}, M.B. Blidaru¹⁰⁹, C. Blume⁶⁹, G. Boca^{28,58}, F. Bock⁹⁸, A. Bogdanov⁹⁵, S. Boi²², J. Bok⁶², L. Boldizsár¹⁴⁶, A. Bolozdynya⁹⁵, M. Bombara³⁸, P.M. Bond³⁴, G. Bonomi^{141,58}, H. Borel¹³⁹, A. Borissov⁸³, H. Bossi¹⁴⁷, E. Botta²⁴, L. Bratrud⁶⁹, P. Braun-Munzinger¹⁰⁹, M. Bregant¹²², M. Broz³⁷, G.E. Bruno^{108,33}, M.D. Buckland¹²⁹, D. Budnikov¹¹⁰, H. Buesching⁶⁹, S. Bufalino³⁰, O. Bugnon¹¹⁶, P. Buhler¹¹⁵, Z. Buthelezi^{73,133}, J.B. Butt¹⁴, A. Bylinkin¹²⁸, S.A. Bysiak¹¹⁹, M. Cai^{27,7}, H. Caines¹⁴⁷, A. Caliva¹⁰⁹, E. Calvo Villar¹¹³, J.M.M. Camacho¹²¹, R.S. Camacho⁴⁵, P. Camerini²³, F.D.M. Canedo¹²², F. Carnesecchi^{34,25}, R. Caron¹³⁹, J. Castillo Castellanos¹³⁹, E.A.R. Casula²², F. Catalano³⁰, C. Ceballos Sanchez⁷⁶, P. Chakraborty⁴⁹, S. Chandra¹⁴², S. Chapeland³⁴, M. Chartier¹²⁹, S. Chattopadhyay¹⁴², S. Chattopadhyay¹¹¹, A. Chauvin²², T.G. Chavez⁴⁵, T. Cheng⁷, C. Cheshkov¹³⁷, B. Cheynis¹³⁷, V. Chibante Barroso³⁴, D.D. Chinellato¹²³, S. Cho⁶², P. Chochula³⁴, P. Christakoglou⁹², C.H. Christensen⁹¹, P. Christiansen⁸², T. Chujo¹³⁵, C. Cicalo⁵⁵, L. Cifarelli²⁵, F. Cindolo⁵⁴, M.R. Ciupek¹⁰⁹, G. Clai^{II,54}, J. Cleymans^{I,125}, F. Colamaria⁵³, J.S. Colburn¹¹², D. Colella^{53,108,33}, A. Collu⁸¹, M. Colucci³⁴, M. Concas^{III,60}, G. Conesa Balbastre⁸⁰, Z. Conesa del Valle⁷⁹, G. Contin²³, J.G. Contreras³⁷, M.L. Coquet¹³⁹, T.M. Cormier⁹⁸, P. Cortese³¹, M.R. Cosentino¹²⁴, F. Costa³⁴, S. Costanza^{28,58}, P. Crochet¹³⁶, R. Cruz-Torres⁸¹, E. Cuautle⁷⁰, P. Cui⁷, L. Cunqueiro⁹⁸, A. Dainese⁵⁷, M.C. Danisch¹⁰⁶, A. Danu⁶⁸, P. Das⁸⁸, P. Das⁴, S. Das⁴, S. Dash⁴⁹, A. De Caro²⁹, G. de Cataldo⁵³, L. De Cilladi²⁴, J. de Cuveland³⁹, A. De Falco²², D. De Gruttola²⁹, N. De Marco⁶⁰, C. De Martin²³, S. De Pasquale²⁹, S. Deb⁵⁰, H.F. Degenhardt¹²², K.R. Deja¹⁴³, L. Dello Stritto²⁹, W. Deng⁷, P. Dhankher¹⁹, D. Di Bari³³, A. Di Mauro³⁴, R.A. Diaz⁸, T. Dietel¹²⁵, Y. Ding^{137,7}, R. Divià³⁴, D.U. Dixit¹⁹, Ø. Djuvsland²¹, U. Dmitrieva⁶⁴, J. Do⁶², A. Dobrin⁶⁸, B. Dönigus⁶⁹, A.K. Dubey¹⁴², A. Dubla^{109,92}, S. Dudi¹⁰², M. Dukhishyam⁸⁸, P. Dupieux¹³⁶, N. Dzalaiova¹³, T.M. Eder¹⁴⁵, R.J. Ehlers⁹⁸, V.N. Eikeland²¹, F. Eisenhut⁶⁹, D. Elia⁵³, B. Erazmus¹¹⁶, F. Ercolessi²⁵, F. Erhardt¹⁰¹, A. Erokhin¹¹⁴, M.R. Ersdal²¹, B. Espagnon⁷⁹, G. Eulisse³⁴, D. Evans¹¹², S. Evdokimov⁹³, L. Fabbietti¹⁰⁷, M. Faggin²⁷, J. Faivre⁸⁰, F. Fan⁷, A. Fantoni⁵², M. Fasel⁹⁸, P. Fecchio³⁰, A. Feliciello⁶⁰, G. Feofilov¹¹⁴, A. Fernández Téllez⁴⁵, A. Ferrero¹³⁹, A. Ferretti²⁴, V.J.G. Feuillard¹⁰⁶, J. Figiel¹¹⁹, S. Filchagin¹¹⁰, D. Finogeev⁶⁴, F.M. Fionda^{55,21}, G. Fiorenza^{34,108}, F. Flor¹²⁶, A.N. Flores¹²⁰, S. Foertsch⁷³, S. Fokin⁹⁰, E. Fragiaco⁶¹, E. Frajna¹⁴⁶, U. Fuchs³⁴, N. Funicello²⁹, C. Furget⁸⁰, A. Furs⁶⁴, J.J. Gaardhøje⁹¹, M. Gagliardi²⁴, A.M. Gago¹¹³, A. Gal¹³⁸, C.D. Galvan¹²¹, P. Ganoti⁸⁶, C. Garabatos¹⁰⁹, J.R.A. Garcia⁴⁵, E. Garcia-Solis¹⁰, K. Garg¹¹⁶, C. Gargiulo³⁴, A. Garibli⁸⁹, K. Garner¹⁴⁵, P. Gasik¹⁰⁹, E.F. Gauger¹²⁰, A. Gautam¹²⁸, M.B. Gay Ducati⁷¹, M. Germain¹¹⁶, P. Ghosh¹⁴², S.K. Ghosh⁴, M. Giacalone²⁵, P. Gianotti⁵², P. Giubellino^{109,60}, P. Giubilato²⁷, A.M.C. Glaenger¹³⁹, P. Glässel¹⁰⁶, D.J.Q. Goh⁸⁴, V. Gonzalez¹⁴⁴, L.H. González-Trueba⁷²,

S. Gorbunov³⁹, M. Gorgon², L. Görlich¹¹⁹, S. Gotovac³⁵, V. Grabski⁷², L.K. Graczykowski¹⁴³, L. Greiner⁸¹, A. Grelli⁶³, C. Grigoras³⁴, V. Grigoriev⁹⁵, S. Grigoryan^{76,1}, F. Grosa^{34,60}, J.F. Grosse-Oetringhaus³⁴, R. Grosso¹⁰⁹, G.G. Guardiano¹²³, R. Guernane⁸⁰, M. Guilbaud¹¹⁶, K. Gulbrandsen⁹¹, T. Gunji¹³⁴, W. Guo⁷, A. Gupta¹⁰³, R. Gupta¹⁰³, S.P. Guzman⁴⁵, L. Gyulai¹⁴⁶, M.K. Habib¹⁰⁹, C. Hadjidakis⁷⁹, H. Hamagaki⁸⁴, M. Hamid⁷, R. Hannigan¹²⁰, M.R. Haque¹⁴³, A. Harlanderova¹⁰⁹, J.W. Harris¹⁴⁷, A. Harton¹⁰, J.A. Hasenbichler³⁴, H. Hassan⁹⁸, D. Hatzifotiadou⁵⁴, P. Hauer⁴³, L.B. Havener¹⁴⁷, S.T. Heckel¹⁰⁷, E. Hellbär¹⁰⁹, H. Helstrup³⁶, T. Herman³⁷, E.G. Hernandez⁴⁵, G. Herrera Corral⁹, F. Herrmann¹⁴⁵, K.F. Hetland³⁶, H. Hillemanns³⁴, C. Hills¹²⁹, B. Hippolyte¹³⁸, B. Hofman⁶³, B. Hohlweger⁹², J. Honermann¹⁴⁵, G.H. Hong¹⁴⁸, D. Horak³⁷, S. Hornung¹⁰⁹, A. Horzyk², R. Hosokawa¹⁵, Y. Hou⁷, P. Hristov³⁴, C. Hughes¹³², P. Huhn⁶⁹, L.M. Huhta¹²⁷, C.V. Hulse⁷⁹, T.J. Humanic⁹⁹, H. Hushnud¹¹¹, L.A. Husova¹⁴⁵, A. Hutson¹²⁶, J.P. Iddon^{34,129}, R. Ilkaev¹¹⁰, H. Ilyas¹⁴, M. Inaba¹³⁵, G.M. Innocenti³⁴, M. Ippolitov⁹⁰, A. Isakov⁹⁷, T. Isidori¹²⁸, M.S. Islam¹¹¹, M. Ivanov¹⁰⁹, V. Ivanov¹⁰⁰, V. Izucheev⁹³, M. Jablonski², B. Jacak⁸¹, N. Jacazio³⁴, P.M. Jacobs⁸¹, S. Jadlovska¹¹⁸, J. Jadlovsky¹¹⁸, S. Jaelani⁶³, C. Jahnke^{123,122}, M.J. Jakubowska¹⁴³, A. Jalotra¹⁰³, M.A. Janik¹⁴³, T. Janson⁷⁵, M. Jercic¹⁰¹, O. Jevons¹¹², A.A.P. Jimenez⁷⁰, F. Jonas^{98,145}, P.G. Jones¹¹², J.M. Jowett^{34,109}, J. Jung⁶⁹, M. Jung⁶⁹, A. Junique³⁴, A. Jusko¹¹², J. Kaewjai¹¹⁷, P. Kalinak⁶⁵, A.S. Kalteyer¹⁰⁹, A. Kalweit³⁴, V. Kaplin⁹⁵, A. Karasu Uysal⁷⁸, D. Karatovic¹⁰¹, O. Karavichev⁶⁴, T. Karavicheva⁶⁴, P. Karczmarczyk¹⁴³, E. Karpechev⁶⁴, V. Kashyap⁸⁸, A. Kazantsev⁹⁰, U. Kebschull⁷⁵, R. Keidel⁴⁷, D.L.D. Keijdener⁶³, M. Keil³⁴, B. Ketzer⁴³, Z. Khabanova⁹², A.M. Khan⁷, S. Khan¹⁶, A. Khanzadeev¹⁰⁰, Y. Kharlov^{93,83}, A. Khatun¹⁶, A. Khuntia¹¹⁹, B. Kileng³⁶, B. Kim^{17,62}, C. Kim¹⁷, D.J. Kim¹²⁷, E.J. Kim⁷⁴, J. Kim¹⁴⁸, J.S. Kim⁴¹, J. Kim¹⁰⁶, J. Kim⁷⁴, M. Kim¹⁰⁶, S. Kim¹⁸, T. Kim¹⁴⁸, S. Kirsch⁶⁹, I. Kisel³⁹, S. Kiselev⁹⁴, A. Kisiel¹⁴³, J.P. Kitowski², J.L. Klay⁶, J. Klein³⁴, S. Klein⁸¹, C. Klein-Bösing¹⁴⁵, M. Kleiner⁶⁹, T. Klemenz¹⁰⁷, A. Kluge³⁴, A.G. Knospe¹²⁶, C. Kobdaj¹¹⁷, M.K. Köhler¹⁰⁶, T. Kollegger¹⁰⁹, A. Kondratyev⁷⁶, N. Kondratyeva⁹⁵, E. Kondratyuk⁹³, J. König⁶⁹, S.A. Königstorfer¹⁰⁷, P.J. Konopka³⁴, G. Kornakov¹⁴³, S.D. Koryciak², A. Kotliarov⁹⁷, O. Kovalenko⁸⁷, V. Kovalenko¹¹⁴, M. Kowalski¹¹⁹, I. Králik⁶⁵, A. Kravčáková³⁸, L. Kreis¹⁰⁹, M. Krivda^{112,65}, F. Krizek⁹⁷, K. Krizkova Gajdosova³⁷, M. Kroesen¹⁰⁶, M. Krüger⁶⁹, E. Kryshen¹⁰⁰, M. Krzewicki³⁹, V. Kučera³⁴, C. Kuhn¹³⁸, P.G. Kuijjer⁹², T. Kumaoka¹³⁵, D. Kumar¹⁴², L. Kumar¹⁰², N. Kumar¹⁰², S. Kundu³⁴, P. Kurashvili⁸⁷, A. Kurepin⁶⁴, A.B. Kurepin⁶⁴, A. Kuryakin¹¹⁰, S. Kuschpil⁹⁷, J. Kvapil¹¹², M.J. Kweon⁶², J.Y. Kwon⁶², Y. Kwon¹⁴⁸, S.L. La Pointe³⁹, P. La Rocca²⁶, Y.S. Lai⁸¹, A. Lakrathok¹¹⁷, M. Lamanna³⁴, R. Langoy¹³¹, K. Lapidus³⁴, P. Larionov^{34,52}, E. Laudi³⁴, L. Lautner^{34,107}, R. Lavicka^{115,37}, T. Lazareva¹¹⁴, R. Lea^{141,23,58}, J. Lehrbach³⁹, R.C. Lemmon⁹⁶, I. León Monzón¹²¹, E.D. Lesser¹⁹, M. Lettrich^{34,107}, P. Lévai¹⁴⁶, X. Li¹¹, X.L. Li⁷, J. Lien¹³¹, R. Lietava¹¹², B. Lim¹⁷, S.H. Lim¹⁷, V. Lindenstruth³⁹, A. Lindner⁴⁸, C. Lippmann¹⁰⁹, A. Liu¹⁹, D.H. Liu⁷, J. Liu¹²⁹, I.M. Lofnes²¹, V. Loginov⁹⁵, C. Loizides⁹⁸, P. Loncar³⁵, J.A. Lopez¹⁰⁶, X. Lopez¹³⁶, E. López Torres⁸, J.R. Luhder¹⁴⁵, M. Lunardon²⁷, G. Luparello⁶¹, Y.G. Ma⁴⁰, A. Maevskaya⁶⁴, M. Mager³⁴, T. Mahmoud⁴³, A. Maire¹³⁸, M. Malaev¹⁰⁰, N.M. Malik¹⁰³, Q.W. Malik²⁰, S.K. Malik¹⁰³, L. Malinina^{IV,76}, D. Mal'Kevich⁹⁴, N. Mallick⁵⁰, G. Mandaglio^{32,56}, V. Manko⁹⁰, F. Manso¹³⁶, V. Manzari⁵³, Y. Mao⁷, G.V. Margagliotti²³, A. Margotti⁵⁴, A. Marín¹⁰⁹, C. Markert¹²⁰, M. Marquard⁶⁹, N.A. Martin¹⁰⁶, P. Martinengo³⁴, J.L. Martinez¹²⁶, M.I. Martínez⁴⁵, G. Martínez García¹¹⁶, S. Masciocchi¹⁰⁹, M. Maserà²⁴, A. Masoni⁵⁵, L. Massacrier⁷⁹, A. Mastroserio^{140,53}, A.M. Mathis¹⁰⁷, O. Matonoha⁸², P.F.T. Matuoka¹²², A. Matyja¹¹⁹, C. Mayer¹¹⁹, A.L. Mazuecos³⁴, F. Mazzaschi²⁴, M. Mazzilli³⁴, M.A. Mazzoni^{I,59}, J.E. Mdhluhi¹³³, A.F. Mechler⁶⁹, Y. Melikyan⁶⁴, A. Menchaca-Rocha⁷², E. Meninno^{115,29}, A.S. Menon¹²⁶, M. Meres¹³, S. Mhlanga^{125,73}, Y. Miake¹³⁵, L. Micheletti⁶⁰, L.C. Migliorin¹³⁷, D.L. Mihaylov¹⁰⁷, K. Mikhaylov^{76,94}, A.N. Mishra¹⁴⁶, D. Miśkowiec¹⁰⁹, A. Modak⁴, A.P. Mohanty⁶³, B. Mohanty⁸⁸, M. Mohisin Khan^{V,16}, M.A. Molander⁴⁴, Z. Moravcova⁹¹, C. Mordasini¹⁰⁷, D.A. Moreira De Godoy¹⁴⁵, I. Morozov⁶⁴, A. Morsch³⁴, T. Mrnjavac³⁴, V. Muccifora⁵², E. Mudnic³⁵, D. Mühlheim¹⁴⁵, S. Muhuri¹⁴², J.D. Mulligan⁸¹, A. Mulliri²², M.G. Munhoz¹²², R.H. Munzer⁶⁹, H. Murakami¹³⁴, S. Murray¹²⁵, L. Musa³⁴, J. Musinsky⁶⁵, J.W. Myrcha¹⁴³, B. Naik^{133,49}, R. Nair⁸⁷, B.K. Nandi⁴⁹, R. Nania⁵⁴, E. Nappi⁵³,

A.F. Nassirpour⁸², A. Nath¹⁰⁶, C. Nattrass¹³², A. Neagu²⁰, L. Nellen⁷⁰, S.V. Nesbo³⁶, G. Neskovic³⁹, D. Nesterov¹¹⁴, B.S. Nielsen⁹¹, S. Nikolaev⁹⁰, S. Nikulin⁹⁰, V. Nikulin¹⁰⁰, F. Noferini⁵⁴, S. Noh¹², P. Nomokonov⁷⁶, J. Norman¹²⁹, N. Novitzky¹³⁵, P. Nowakowski¹⁴³, A. Nyanin⁹⁰, J. Nystrand²¹, M. Ogino⁸⁴, A. Ohlson⁸², V.A. Okorokov⁹⁵, J. Oleniacz¹⁴³, A.C. Oliveira Da Silva¹³², M.H. Oliver¹⁴⁷, A. Onnerstad¹²⁷, C. Oppedisano⁶⁰, A. Ortiz Velasquez⁷⁰, T. Osako⁴⁶, A. Oskarsson⁸², J. Otwinowski¹¹⁹, M. Oya⁴⁶, K. Oyama⁸⁴, Y. Pachmayer¹⁰⁶, S. Padhan⁴⁹, D. Pagano^{141,58}, G. Paic⁷⁰, A. Palasciano⁵³, J. Pan¹⁴⁴, S. Panebianco¹³⁹, J. Park⁶², J.E. Parkkila¹²⁷, S.P. Pathak¹²⁶, R.N. Patra^{103,34}, B. Paul²², H. Pei⁷, T. Peitzmann⁶³, X. Peng⁷, L.G. Pereira⁷¹, H. Pereira Da Costa¹³⁹, D. Peresunko^{90,83}, G.M. Perez⁸, S. Perrin¹³⁹, Y. Pestov⁵, V. Petráček³⁷, M. Petrovici⁴⁸, R.P. Pezzi^{116,71}, S. Piano⁶¹, M. Pikna¹³, P. Pillot¹¹⁶, O. Pinazza^{54,34}, L. Pinsky¹²⁶, C. Pinto²⁶, S. Pisano⁵², M. Płoskoń⁸¹, M. Planinic¹⁰¹, F. Pliquett⁶⁹, M.G. Poghosyan⁹⁸, B. Polichtchouk⁹³, S. Politano³⁰, N. Poljak¹⁰¹, A. Pop⁴⁸, S. Porteboeuf-Houssais¹³⁶, J. Porter⁸¹, V. Pozdniakov⁷⁶, S.K. Prasad⁴, R. Preghenella⁵⁴, F. Prino⁶⁰, C.A. Pruneau¹⁴⁴, I. Pshenichnov⁶⁴, M. Puccio³⁴, S. Qiu⁹², L. Quaglia²⁴, R.E. Quishpe¹²⁶, S. Ragoni¹¹², A. Rakotozafindrabe¹³⁹, L. Ramello³¹, F. Rami¹³⁸, S.A.R. Ramirez⁴⁵, A.G.T. Ramos³³, T.A. Rancien⁸⁰, R. Raniwala¹⁰⁴, S. Raniwala¹⁰⁴, S.S. Räsänen⁴⁴, R. Rath⁵⁰, I. Ravasenga⁹², K.F. Read^{98,132}, A.R. Redelbach³⁹, K. Redlich^{VI,87}, A. Rehman²¹, P. Reichelt⁶⁹, F. Reidt³⁴, H.A. Reme-ness³⁶, Z. Rescakova³⁸, K. Reygers¹⁰⁶, A. Riabov¹⁰⁰, V. Riabov¹⁰⁰, T. Richert⁸², M. Richter²⁰, W. Riegler³⁴, F. Riggi²⁶, C. Ristea⁶⁸, M. Rodríguez Cahuantzi⁴⁵, K. Røed²⁰, R. Rogalev⁹³, E. Rogochaya⁷⁶, T.S. Rogoschinski⁶⁹, D. Rohr³⁴, D. Röhrich²¹, P.F. Rojas⁴⁵, P.S. Rokita¹⁴³, F. Ronchetti⁵², A. Rosano^{32,56}, E.D. Rosas⁷⁰, A. Rossi⁵⁷, A. Roy⁵⁰, P. Roy¹¹¹, S. Roy⁴⁹, N. Rubini²⁵, O.V. Rueda⁸², D. Ruggiano¹⁴³, R. Rui²³, B. Rumyantsev⁷⁶, P.G. Russek², R. Russo⁹², A. Rustamov⁸⁹, E. Ryabinkin⁹⁰, Y. Ryabov¹⁰⁰, A. Rybicki¹¹⁹, H. Rytönen¹²⁷, W. Rzesza¹⁴³, O.A.M. Saariimäki⁴⁴, R. Sadek¹¹⁶, S. Sadovsky⁹³, J. Saetre²¹, K. Šafařík³⁷, S.K. Saha¹⁴², S. Saha⁸⁸, B. Sahoo⁴⁹, P. Sahoo⁴⁹, R. Sahoo⁵⁰, S. Sahoo⁶⁶, D. Sahu⁵⁰, P.K. Sahu⁶⁶, J. Saini¹⁴², S. Sakai¹³⁵, M.P. Salvan¹⁰⁹, S. Sambyal¹⁰³, V. Samsonov^{I,100,95}, D. Sarkar¹⁴⁴, N. Sarkar¹⁴², P. Sarma⁴², V.M. Sarti¹⁰⁷, M.H.P. Sas¹⁴⁷, J. Schambach⁹⁸, H.S. Scheid⁶⁹, C. Schiaua⁴⁸, R. Schicker¹⁰⁶, A. Schmah¹⁰⁶, C. Schmidt¹⁰⁹, H.R. Schmidt¹⁰⁵, M.O. Schmidt^{34,106}, M. Schmidt¹⁰⁵, N.V. Schmidt^{98,69}, A.R. Schmier¹³², R. Schotter¹³⁸, J. Schukraft³⁴, K. Schwarz¹⁰⁹, K. Schweda¹⁰⁹, G. Scioli²⁵, E. Scapparini⁶⁰, J.E. Seger¹⁵, Y. Sekiguchi¹³⁴, D. Sekihata¹³⁴, I. Selyuzhenkov^{109,95}, S. Senyukov¹³⁸, J.J. Seo⁶², D. Serebryakov⁶⁴, L. Šerkšnytė¹⁰⁷, A. Sevcenco⁶⁸, T.J. Shaba⁷³, A. Shabanov⁶⁴, A. Shabetai¹¹⁶, R. Shahoyan³⁴, W. Shaikh¹¹¹, A. Shangaraev⁹³, A. Sharma¹⁰², H. Sharma¹¹⁹, M. Sharma¹⁰³, N. Sharma¹⁰², S. Sharma¹⁰³, U. Sharma¹⁰³, O. Sheibani¹²⁶, K. Shigaki⁴⁶, M. Shimomura⁸⁵, S. Shirinkin⁹⁴, Q. Shou⁴⁰, Y. Sibiriak⁹⁰, S. Siddhanta⁵⁵, T. Siemiarczuk⁸⁷, T.F. Silva¹²², D. Silvermyr⁸², T. Simantathammakul¹¹⁷, G. Simonetti³⁴, B. Singh¹⁰⁷, R. Singh⁸⁸, R. Singh¹⁰³, R. Singh⁵⁰, V.K. Singh¹⁴², V. Singhal¹⁴², T. Sinha¹¹¹, B. Sitar¹³, M. Sitta³¹, T.B. Skaali²⁰, G. Skorodumovs¹⁰⁶, M. Slupecki⁴⁴, N. Smirnov¹⁴⁷, R.J.M. Snellings⁶³, C. Soncco¹¹³, J. Song¹²⁶, A. Songmoolnak¹¹⁷, F. Soramel²⁷, S. Sorensen¹³², I. Sputowska¹¹⁹, J. Stachel¹⁰⁶, I. Stan⁶⁸, P.J. Steffanic¹³², S.F. Stiefelmaier¹⁰⁶, D. Stocco¹¹⁶, I. Storehaug²⁰, M.M. Stortvedt³⁶, P. Stratmann¹⁴⁵, C.P. Stylianidis⁹², A.A.P. Suaide¹²², C. Suire⁷⁹, M. Sukhanov⁶⁴, M. Suljic³⁴, R. Sultanov⁹⁴, V. Sumberia¹⁰³, S. Sumowidagdo⁵¹, S. Swain⁶⁶, A. Szabo¹³, I. Szarka¹³, U. Tabassam¹⁴, S.F. Taghavi¹⁰⁷, G. TAILLEPIED¹³⁶, J. Takahashi¹²³, G.J. Tambave²¹, S. Tang^{136,7}, Z. Tang¹³⁰, J.D. Tapia Takaki^{VII,128}, M. Tarhini¹¹⁶, M.G. Tarzila⁴⁸, A. Tauro³⁴, G. Tejada Muñoz⁴⁵, A. Telesca³⁴, L. Terlizzi²⁴, C. Terrevoli¹²⁶, G. Tersimonov³, S. Thakur¹⁴², D. Thomas¹²⁰, R. Tieulent¹³⁷, A. Tikhonov⁶⁴, A.R. Timmins¹²⁶, M. Tkacik¹¹⁸, A. Toia⁶⁹, N. Topilskaya⁶⁴, M. Toppi⁵², F. Torales-Acosta¹⁹, T. Tork⁷⁹, S.R. Torres³⁷, A. Trifiro^{32,56}, S. Tripathy^{54,70}, T. Tripathy⁴⁹, S. Trogolo^{34,27}, V. Trubnikov³, W.H. Trzaska¹²⁷, T.P. Trzcinski¹⁴³, A. Tumkin¹¹⁰, R. Turrisi⁵⁷, T.S. Tveter²⁰, K. Ullaland²¹, A. Uras¹³⁷, M. Urioni^{58,141}, G.L. Usai²², M. Vala³⁸, N. Valle^{28,58}, S. Vallero⁶⁰, L.V.R. van Doremalen⁶³, M. van Leeuwen⁹², P. Vande Vyvre³⁴, D. Varga¹⁴⁶, Z. Varga¹⁴⁶, M. Varga-Kofarago¹⁴⁶, M. Vasileiou⁸⁶, A. Vasiliev⁹⁰, O. Vázquez Doce^{52,107}, V. Vechernin¹¹⁴, E. Vercellin²⁴, S. Vergara Limón⁴⁵, L. Vermunt⁶³, R. Vértesi¹⁴⁶, M. Verweij⁶³, L. Vickovic³⁵, Z. Vilakazi¹³³, O. Villalobos Baillie¹¹²,

G. VINO⁵³, A. Vinogradov⁹⁰, T. Virgili²⁹, V. Viskavicius⁹¹, A. Vodopyanov⁷⁶, B. Volkel^{34,106}, M.A. Völkl¹⁰⁶, K. Voloshin⁹⁴, S.A. Voloshin¹⁴⁴, G. Volpe³³, B. von Haller³⁴, I. Vorobyev¹⁰⁷, D. Voscek¹¹⁸, N. Vozniuk⁶⁴, J. Vrláková³⁸, B. Wagner²¹, C. Wang⁴⁰, D. Wang⁴⁰, M. Weber¹¹⁵, R.J.G.V. Weelden⁹², A. Wegrzynek³⁴, S.C. Wenzel³⁴, J.P. Wessels¹⁴⁵, J. Wiechula⁶⁹, J. Wikne²⁰, G. Wilk⁸⁷, J. Wilkinson¹⁰⁹, G.A. Willems¹⁴⁵, B. Windelband¹⁰⁶, M. Winn¹³⁹, W.E. Witt¹³², J.R. Wright¹²⁰, W. Wu⁴⁰, Y. Wu¹³⁰, R. Xu⁷, A.K. Yadav¹⁴², S. Yalcin⁷⁸, Y. Yamaguchi⁴⁶, K. Yamakawa⁴⁶, S. Yang²¹, S. Yano⁴⁶, Z. Yin⁷, I.-K. Yoo¹⁷, J.H. Yoon⁶², S. Yuan²¹, A. Yuncu¹⁰⁶, V. Zaccolo²³, C. Zampolli³⁴, H.J.C. Zanoli⁶³, N. Zardoshti³⁴, A. Zarochentsev¹¹⁴, P. Závada⁶⁷, N. Zaviyalov¹¹⁰, M. Zhalov¹⁰⁰, B. Zhang⁷, S. Zhang⁴⁰, X. Zhang⁷, Y. Zhang¹³⁰, V. Zhrebchevskii¹¹⁴, Y. Zhi¹¹, N. Zhigareva⁹⁴, D. Zhou⁷, Y. Zhou⁹¹, J. Zhu^{109,7}, Y. Zhu⁷, G. Zinovjev³, N. Zurlo^{141,58}

Affiliation Notes

^I Deceased

^{II} Also at: Italian National Agency for New Technologies, Energy and Sustainable Economic Development (ENEA), Bologna, Italy

^{III} Also at: Dipartimento DET del Politecnico di Torino, Turin, Italy

^{IV} Also at: M.V. Lomonosov Moscow State University, D.V. Skobeltsyn Institute of Nuclear Physics, Moscow, Russia

^V Also at: Department of Applied Physics, Aligarh Muslim University, Aligarh, India

^{VI} Also at: Institute of Theoretical Physics, University of Wrocław, Poland

^{VII} Also at: University of Kansas, Lawrence, Kansas, United States

Collaboration Institutes

¹ A.I. Alikhanyan National Science Laboratory (Yerevan Physics Institute) Foundation, Yerevan, Armenia

² AGH University of Science and Technology, Cracow, Poland

³ Bogolyubov Institute for Theoretical Physics, National Academy of Sciences of Ukraine, Kiev, Ukraine

⁴ Bose Institute, Department of Physics and Centre for Astroparticle Physics and Space Science (CAPSS), Kolkata, India

⁵ Budker Institute for Nuclear Physics, Novosibirsk, Russia

⁶ California Polytechnic State University, San Luis Obispo, California, United States

⁷ Central China Normal University, Wuhan, China

⁸ Centro de Aplicaciones Tecnológicas y Desarrollo Nuclear (CEADEN), Havana, Cuba

⁹ Centro de Investigación y de Estudios Avanzados (CINVESTAV), Mexico City and Mérida, Mexico

¹⁰ Chicago State University, Chicago, Illinois, United States

¹¹ China Institute of Atomic Energy, Beijing, China

¹² Chungbuk National University, Cheongju, Republic of Korea

¹³ Comenius University Bratislava, Faculty of Mathematics, Physics and Informatics, Bratislava, Slovakia

¹⁴ COMSATS University Islamabad, Islamabad, Pakistan

¹⁵ Creighton University, Omaha, Nebraska, United States

¹⁶ Department of Physics, Aligarh Muslim University, Aligarh, India

¹⁷ Department of Physics, Pusan National University, Pusan, Republic of Korea

¹⁸ Department of Physics, Sejong University, Seoul, Republic of Korea

¹⁹ Department of Physics, University of California, Berkeley, California, United States

- ²⁰ Department of Physics, University of Oslo, Oslo, Norway
- ²¹ Department of Physics and Technology, University of Bergen, Bergen, Norway
- ²² Dipartimento di Fisica dell'Università and Sezione INFN, Cagliari, Italy
- ²³ Dipartimento di Fisica dell'Università and Sezione INFN, Trieste, Italy
- ²⁴ Dipartimento di Fisica dell'Università and Sezione INFN, Turin, Italy
- ²⁵ Dipartimento di Fisica e Astronomia dell'Università and Sezione INFN, Bologna, Italy
- ²⁶ Dipartimento di Fisica e Astronomia dell'Università and Sezione INFN, Catania, Italy
- ²⁷ Dipartimento di Fisica e Astronomia dell'Università and Sezione INFN, Padova, Italy
- ²⁸ Dipartimento di Fisica e Nucleare e Teorica, Università di Pavia, Pavia, Italy
- ²⁹ Dipartimento di Fisica 'E.R. Caianiello' dell'Università and Gruppo Collegato INFN, Salerno, Italy
- ³⁰ Dipartimento DISAT del Politecnico and Sezione INFN, Turin, Italy
- ³¹ Dipartimento di Scienze e Innovazione Tecnologica dell'Università del Piemonte Orientale and INFN Sezione di Torino, Alessandria, Italy
- ³² Dipartimento di Scienze MIFT, Università di Messina, Messina, Italy
- ³³ Dipartimento Interateneo di Fisica 'M. Merlin' and Sezione INFN, Bari, Italy
- ³⁴ European Organization for Nuclear Research (CERN), Geneva, Switzerland
- ³⁵ Faculty of Electrical Engineering, Mechanical Engineering and Naval Architecture, University of Split, Split, Croatia
- ³⁶ Faculty of Engineering and Science, Western Norway University of Applied Sciences, Bergen, Norway
- ³⁷ Faculty of Nuclear Sciences and Physical Engineering, Czech Technical University in Prague, Prague, Czech Republic
- ³⁸ Faculty of Science, P.J. Šafárik University, Košice, Slovakia
- ³⁹ Frankfurt Institute for Advanced Studies, Johann Wolfgang Goethe-Universität Frankfurt, Frankfurt, Germany
- ⁴⁰ Fudan University, Shanghai, China
- ⁴¹ Gangneung-Wonju National University, Gangneung, Republic of Korea
- ⁴² Gauhati University, Department of Physics, Guwahati, India
- ⁴³ Helmholtz-Institut für Strahlen- und Kernphysik, Rheinische Friedrich-Wilhelms-Universität Bonn, Bonn, Germany
- ⁴⁴ Helsinki Institute of Physics (HIP), Helsinki, Finland
- ⁴⁵ High Energy Physics Group, Universidad Autónoma de Puebla, Puebla, Mexico
- ⁴⁶ Hiroshima University, Hiroshima, Japan
- ⁴⁷ Hochschule Worms, Zentrum für Technologietransfer und Telekommunikation (ZTT), Worms, Germany
- ⁴⁸ Horia Hulubei National Institute of Physics and Nuclear Engineering, Bucharest, Romania
- ⁴⁹ Indian Institute of Technology Bombay (IIT), Mumbai, India
- ⁵⁰ Indian Institute of Technology Indore, Indore, India
- ⁵¹ Indonesian Institute of Sciences, Jakarta, Indonesia
- ⁵² INFN, Laboratori Nazionali di Frascati, Frascati, Italy
- ⁵³ INFN, Sezione di Bari, Bari, Italy
- ⁵⁴ INFN, Sezione di Bologna, Bologna, Italy
- ⁵⁵ INFN, Sezione di Cagliari, Cagliari, Italy
- ⁵⁶ INFN, Sezione di Catania, Catania, Italy
- ⁵⁷ INFN, Sezione di Padova, Padova, Italy
- ⁵⁸ INFN, Sezione di Pavia, Pavia, Italy
- ⁵⁹ INFN, Sezione di Roma, Rome, Italy
- ⁶⁰ INFN, Sezione di Torino, Turin, Italy
- ⁶¹ INFN, Sezione di Trieste, Trieste, Italy
- ⁶² Inha University, Incheon, Republic of Korea

- ⁶³ Institute for Gravitational and Subatomic Physics (GRASP), Utrecht University/Nikhef, Utrecht, Netherlands
- ⁶⁴ Institute for Nuclear Research, Academy of Sciences, Moscow, Russia
- ⁶⁵ Institute of Experimental Physics, Slovak Academy of Sciences, Košice, Slovakia
- ⁶⁶ Institute of Physics, Homi Bhabha National Institute, Bhubaneswar, India
- ⁶⁷ Institute of Physics of the Czech Academy of Sciences, Prague, Czech Republic
- ⁶⁸ Institute of Space Science (ISS), Bucharest, Romania
- ⁶⁹ Institut für Kernphysik, Johann Wolfgang Goethe-Universität Frankfurt, Frankfurt, Germany
- ⁷⁰ Instituto de Ciencias Nucleares, Universidad Nacional Autónoma de México, Mexico City, Mexico
- ⁷¹ Instituto de Física, Universidade Federal do Rio Grande do Sul (UFRGS), Porto Alegre, Brazil
- ⁷² Instituto de Física, Universidad Nacional Autónoma de México, Mexico City, Mexico
- ⁷³ iThemba LABS, National Research Foundation, Somerset West, South Africa
- ⁷⁴ Jeonbuk National University, Jeonju, Republic of Korea
- ⁷⁵ Johann-Wolfgang-Goethe Universität Frankfurt Institut für Informatik, Fachbereich Informatik und Mathematik, Frankfurt, Germany
- ⁷⁶ Joint Institute for Nuclear Research (JINR), Dubna, Russia
- ⁷⁷ Korea Institute of Science and Technology Information, Daejeon, Republic of Korea
- ⁷⁸ KTO Karatay University, Konya, Turkey
- ⁷⁹ Laboratoire de Physique des 2 Infinis, Irène Joliot-Curie, Orsay, France
- ⁸⁰ Laboratoire de Physique Subatomique et de Cosmologie, Université Grenoble-Alpes, CNRS-IN2P3, Grenoble, France
- ⁸¹ Lawrence Berkeley National Laboratory, Berkeley, California, United States
- ⁸² Lund University Department of Physics, Division of Particle Physics, Lund, Sweden
- ⁸³ Moscow Institute for Physics and Technology, Moscow, Russia
- ⁸⁴ Nagasaki Institute of Applied Science, Nagasaki, Japan
- ⁸⁵ Nara Women's University (NWU), Nara, Japan
- ⁸⁶ National and Kapodistrian University of Athens, School of Science, Department of Physics, Athens, Greece
- ⁸⁷ National Centre for Nuclear Research, Warsaw, Poland
- ⁸⁸ National Institute of Science Education and Research, Homi Bhabha National Institute, Jatni, India
- ⁸⁹ National Nuclear Research Center, Baku, Azerbaijan
- ⁹⁰ National Research Centre Kurchatov Institute, Moscow, Russia
- ⁹¹ Niels Bohr Institute, University of Copenhagen, Copenhagen, Denmark
- ⁹² Nikhef, National institute for subatomic physics, Amsterdam, Netherlands
- ⁹³ NRC Kurchatov Institute IHEP, Protvino, Russia
- ⁹⁴ NRC «Kurchatov» Institute - ITEP, Moscow, Russia
- ⁹⁵ NRNU Moscow Engineering Physics Institute, Moscow, Russia
- ⁹⁶ Nuclear Physics Group, STFC Daresbury Laboratory, Daresbury, United Kingdom
- ⁹⁷ Nuclear Physics Institute of the Czech Academy of Sciences, Řež u Prahy, Czech Republic
- ⁹⁸ Oak Ridge National Laboratory, Oak Ridge, Tennessee, United States
- ⁹⁹ Ohio State University, Columbus, Ohio, United States
- ¹⁰⁰ Petersburg Nuclear Physics Institute, Gatchina, Russia
- ¹⁰¹ Physics department, Faculty of science, University of Zagreb, Zagreb, Croatia
- ¹⁰² Physics Department, Panjab University, Chandigarh, India
- ¹⁰³ Physics Department, University of Jammu, Jammu, India
- ¹⁰⁴ Physics Department, University of Rajasthan, Jaipur, India
- ¹⁰⁵ Physikalisches Institut, Eberhard-Karls-Universität Tübingen, Tübingen, Germany
- ¹⁰⁶ Physikalisches Institut, Ruprecht-Karls-Universität Heidelberg, Heidelberg, Germany
- ¹⁰⁷ Physik Department, Technische Universität München, Munich, Germany
- ¹⁰⁸ Politecnico di Bari and Sezione INFN, Bari, Italy

- ¹⁰⁹ Research Division and ExtreMe Matter Institute EMMI, GSI Helmholtzzentrum für Schwerionenforschung GmbH, Darmstadt, Germany
- ¹¹⁰ Russian Federal Nuclear Center (VNIIEF), Sarov, Russia
- ¹¹¹ Saha Institute of Nuclear Physics, Homi Bhabha National Institute, Kolkata, India
- ¹¹² School of Physics and Astronomy, University of Birmingham, Birmingham, United Kingdom
- ¹¹³ Sección Física, Departamento de Ciencias, Pontificia Universidad Católica del Perú, Lima, Peru
- ¹¹⁴ St. Petersburg State University, St. Petersburg, Russia
- ¹¹⁵ Stefan Meyer Institut für Subatomare Physik (SMI), Vienna, Austria
- ¹¹⁶ SUBATECH, IMT Atlantique, Université de Nantes, CNRS-IN2P3, Nantes, France
- ¹¹⁷ Suranaree University of Technology, Nakhon Ratchasima, Thailand
- ¹¹⁸ Technical University of Košice, Košice, Slovakia
- ¹¹⁹ The Henryk Niewodniczanski Institute of Nuclear Physics, Polish Academy of Sciences, Cracow, Poland
- ¹²⁰ The University of Texas at Austin, Austin, Texas, United States
- ¹²¹ Universidad Autónoma de Sinaloa, Culiacán, Mexico
- ¹²² Universidade de São Paulo (USP), São Paulo, Brazil
- ¹²³ Universidade Estadual de Campinas (UNICAMP), Campinas, Brazil
- ¹²⁴ Universidade Federal do ABC, Santo Andre, Brazil
- ¹²⁵ University of Cape Town, Cape Town, South Africa
- ¹²⁶ University of Houston, Houston, Texas, United States
- ¹²⁷ University of Jyväskylä, Jyväskylä, Finland
- ¹²⁸ University of Kansas, Lawrence, Kansas, United States
- ¹²⁹ University of Liverpool, Liverpool, United Kingdom
- ¹³⁰ University of Science and Technology of China, Hefei, China
- ¹³¹ University of South-Eastern Norway, Tonsberg, Norway
- ¹³² University of Tennessee, Knoxville, Tennessee, United States
- ¹³³ University of the Witwatersrand, Johannesburg, South Africa
- ¹³⁴ University of Tokyo, Tokyo, Japan
- ¹³⁵ University of Tsukuba, Tsukuba, Japan
- ¹³⁶ Université Clermont Auvergne, CNRS/IN2P3, LPC, Clermont-Ferrand, France
- ¹³⁷ Université de Lyon, CNRS/IN2P3, Institut de Physique des 2 Infinis de Lyon, Lyon, France
- ¹³⁸ Université de Strasbourg, CNRS, IPHC UMR 7178, F-67000 Strasbourg, France, Strasbourg, France
- ¹³⁹ Université Paris-Saclay Centre d'Etudes de Saclay (CEA), IRFU, Département de Physique Nucléaire (DPhN), Saclay, France
- ¹⁴⁰ Università degli Studi di Foggia, Foggia, Italy
- ¹⁴¹ Università di Brescia, Brescia, Italy
- ¹⁴² Variable Energy Cyclotron Centre, Homi Bhabha National Institute, Kolkata, India
- ¹⁴³ Warsaw University of Technology, Warsaw, Poland
- ¹⁴⁴ Wayne State University, Detroit, Michigan, United States
- ¹⁴⁵ Westfälische Wilhelms-Universität Münster, Institut für Kernphysik, Münster, Germany
- ¹⁴⁶ Wigner Research Centre for Physics, Budapest, Hungary
- ¹⁴⁷ Yale University, New Haven, Connecticut, United States
- ¹⁴⁸ Yonsei University, Seoul, Republic of Korea